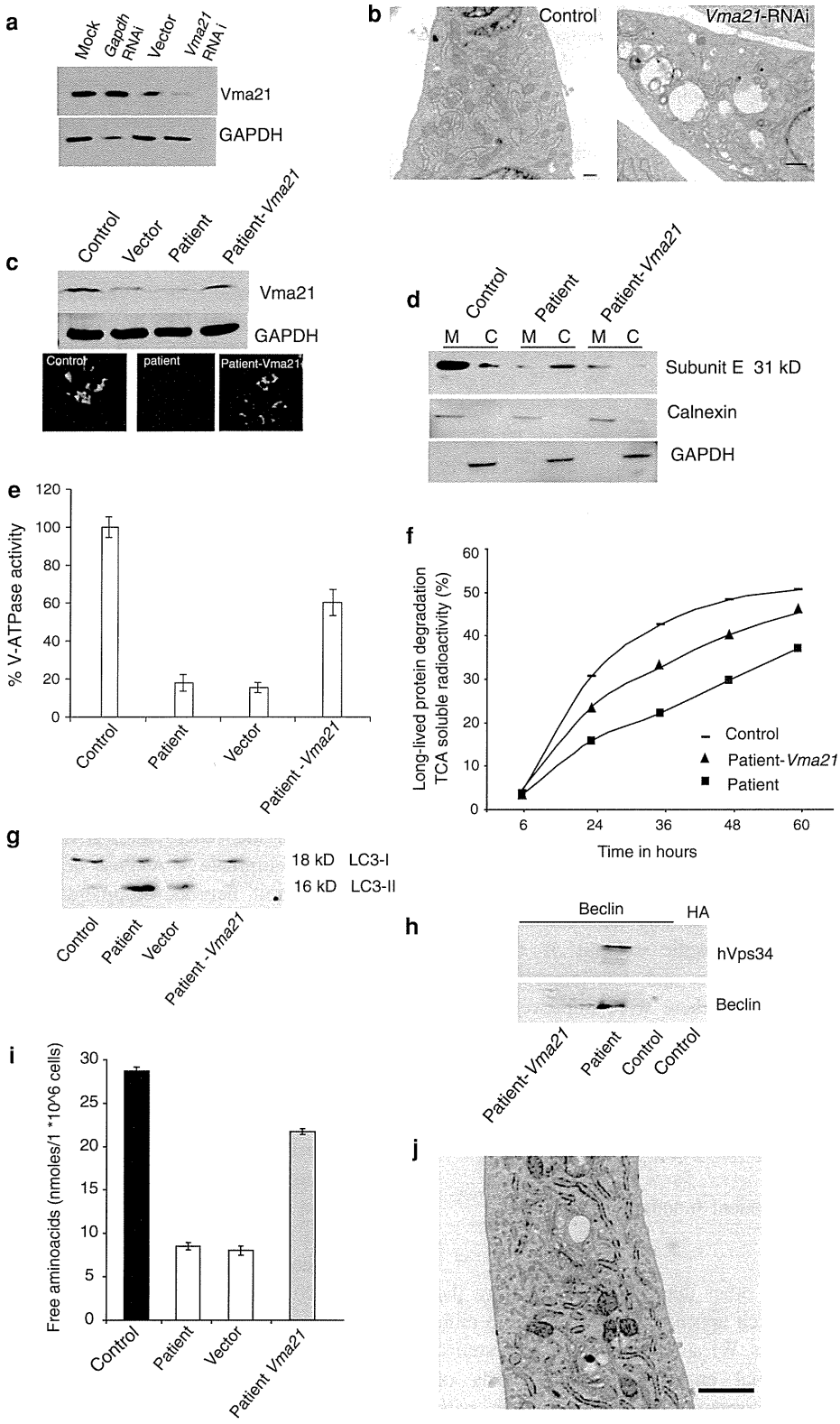
a
Mock
Gapdh RNAi
Vector
Vma21 RNAi
Vma21
GAPDH
b
Control
Vma21-RNAi
c
Control
Vector
Patient
Patient-Vma21
Vma21
GAPDH
Control
patient
Patient-Vma21
d
Control
Patient
Patient-Vma21
M C M C M C
Subunit E 31 kD
Calnexin
GAPDH
e
% V-ATPase activity
120
100
80
60
40
20
0
Control
Patient
Vector
Patient -Vma21
f
Long-lived protein degradation
TCA soluble radioactivity (%)
60
50
40
30
20
10
0
6
24
36
48
60
Time in hours
Control
Patient-Vma21
Patient
g
18 kD LC3-I
16 kD LC3-II
Control
Patient
Vector
Patient -Vma21
h
Beclin
HA
hVps34
Beclin
Patient-Vma21
Patient
Control
Control
i
Free aminoacids (nmoles/1 *10^6 cells)
30
25
20
15
10
5
0
Control
Patient
Vector
Patient Vma21
j

◀**Fig. 9** Downregulating *Vma21* generates XMEA-like vacuolation in normal cells, and restoring *Vma21* mRNA levels in patient cells corrects the XMEA autophagic disturbance phenotypes. **a** Western blot with antibody against Vma21 showing reduced Vma21 in NIH 3T3 cells treated with *VMA21* RNAi; *mock lane* cells treated with transfection reagents with no vectors; *vector lane* same as mock but includes empty vector. **b** Electron micrograph of *Vma21* RNAi-treated NIH 3T3 cells shows typical vacuolation as in XMEA; *left panel* representative cell from empty vector transfection; *right panel* representative cell from *Vma21* siRNA transfection; *bar* 0.5 μm. **c** HIV-mediated expression of Vma21 followed by Western blotting (*top panel*) and immunofluoresence microscopy (*bottom panel*) using the Vma21 antibody; *Control* cell line from unaffected individual with no treatment; *Vector* XMEA cell line treated with empty viral vector; *Patient* XMEA cell line untreated; *Patient-Vma21* XMEA cell line treated with *Vma21* viral vector; retroviral expression method described in Supplement. **d** Improved V-ATPase assembly as verified by normalization of cytosolic Subunit E levels (Western blot with anti-E antibody); *M* membrane fraction and *C* cytosolic fraction. **e** Improved V-ATPase activity. **f** Improved long-lived protein degradation. **g** Correction of LC3. **h** Normalization of beclin and hVps34-beclin-1 interaction; anti-HA antibody immunoprecipitation control. **i** Correction of intracellular free amino acid level. **j** Normalization of cellular morphology and disappearance of autophagic vacuolation; representative patient cell following *Vma21* viral transfection; *bar* 0.5 μm

compensatory upregulation of macroautophagy with which cells achieve the 50 % level. The block in the final stage of autophagy is likely at least in part the driver of the predegradative stages of autophagy that defines this disease. As we here, and others [15, 37], have shown direct inhibition of lysosomal hydrolases with leupeptin leads to mTORC1 inactivation-dependent upregulation of autophagy. Expected outcomes of blocked autophagy are reduced recycling of defective and unneeded proteins, and reduced generation of amino acids through this recycling. Reduced amino acids, specifically leucine, are the most potent inducer of macroautophagy, through inhibition of the mTORC1 pathway. Total cellular amino acids, including leucine, are reduced in XMEA cells by ~50 % and, therefore, the autophagic upregulation in this disease is at least in part due to amino acid insufficiency. This is confirmed by the correction of mTORC1 signaling with replenishment of leucine in the form of leucine esters. A second explanation for the autophagic activation in XMEA comes to light with recent elegant work showing that the V-ATPase, in the lysosomal membrane, plays a central role in the sensing of amino acid levels, and through direct interactions with Rag GTPases regulating the mTORC1 pathway [38]. Reduced V-ATPases would reduce mTORC1 activation, which in turn activates autophagy. This direct function of the V-ATPase in regulating autophagy, like other V-ATPase functions, appears to be only partially eliminated in our patients, as evidenced by the correctability of the autophagic upregulation when an excess of leucine esters is added to the cell media.

Why do amino acids, including leucine, remain low in XMEA cells, despite their abundance in culture media (or through nutrition in the patients), i.e., why do XMEA cells not replenish their amino acids from the media? We speculate that this is a physiological response. If the cells were to fully replace their amino acid shortfalls resulting from the autophagic defect with extrinsic amino acids they would continually acquire net surpluses of proteins which would increasingly tax already strained autophagy. The cells may have adapted to a new homeostasis that allows survival in a starvation-equivalent mode rather than demise through total autophagic failure. Consistent with a reduction in amino acid uptake is our observation that leucine proper which requires active transport, only partially rescues the mTORC1 pathway inactivation in these cells, compared to leucine ester, which does not require active transport. It is, of course, also possible that the putative amino acid transport defect is pathologic, a component of the disease that requires future elucidation.

Increased macroautophagy means increased formation of autolysosomes, but in XMEA each new autolysosome formed faces a degradative block and is slow to progress and disappear. We theorize that increased formation coupled with delayed progression results in vast numbers of autolysosomes, which fusing together form the giant autophagic vacuoles that characterize the disease.

We posited that the autophagic block is a consequence of decreased V-ATPase activity. The possibility exists that it is instead caused by some other effect of the VMA21 mutations unrelated to their effect on the V-ATPase. This is ruled out by the following. Bafilomycin is a specific inhibitor of the V-ATPase. At concentrations above 10 nM, it completely inhibits V-ATPase activity. Between 0.3 and 10 nM it reduces V-ATPase activity to 10–40 % of normal [7], similar to the V-ATPase activity in XMEA. There are several reports in the literature in which, as controls for other experiments, cells of various types were treated with these low concentrations of bafilomycin. This resulted in decreased autophagy, mTORC1 inactivation-dependent activation of macroautophagy, and autolysosome proliferation and autophagic vacuolation [25, 31], which upon review are identical to what we observe in XMEA. V-ATPase blockage, therefore, has the same outcome as VMA21 mutations, confirming that the mutations cause the autophagic defect via their effect on the V-ATPase. The literature also substantiates that decreased V-ATPase causes the autophagic block through raising lysosomal pH. Chloroquine and siramesine are agents that accumulate in lysosomes, raise lysosomal pH, block autophagy, and lead to mTORC1 inactivation-dependent macroautophagy and autophagic vacuolation [25, 31, 33]. Chloroquine is in clinical use as an antimalarial and antirheumatic agent.

Prolonged exposure to chloroquine causes an iatrogenic disease clinically affecting only skeletal muscle, and retina despite the fact that lysosomes of all tissues are affected. This disease is an autophagic vacuolar myopathy that is so similar to XMEA that it is its main pathological differential diagnosis [12, 33]. Finally, that autophagic block is at least in part the cause of the macroautophagic upregulation and autophagic vacuolation, is demonstrated in this study.

Apart from chloroquine myopathy, the differential diagnosis of XMEA includes Danon disease, which results from LAMP2 deficiency [24]. LAMP2 is a lysosomal membrane protein that participates in chaperone-mediated autophagy, lysosome biogenesis, lysosome–autophagosome fusion, and lysosome locomotion along microtubules toward phagosomes [17]. Defects in any or all of these processes could reduce degradative autophagy and underlie the vacuolation in Danon disease. In fact, in the mouse model of this disease, organs with impaired long-lived protein degradation are the ones that exhibit autophagic vacuolation [34]. As such, the pathogenesis of both major forms of vacuolar myopathy, Danon disease, and XMEA would include a block in the degradative phase of autophagy, in Danon disease due to the loss of the above lysosomal functions, in XMEA due to lost V-ATPase activity. We did verify that Danon disease is not associated with V-ATPase deficiency (Supplemental Fig. 13).

Presence of autophagic vacuolation in all XMEA cell types studied to date indicates that the disease is likely subclinically widespread. Why only skeletal muscle is affected clinically is unknown. This does not appear to be due to a greater reduction in V-ATPase activity in muscle compared to other tissues (Fig. 3a, b). The greater autophagic vacuolation in skeletal muscle where 40–80 % of cells are affected [12, 36] compared to the 10 % affected cells in other tissues studied in this work, suggests that skeletal muscle might be reacting more vigorously to the blocked autophagy than other tissues. In fact, macroautophagy in skeletal muscle is characterized by the particularity of a vastly greater macroautophagic response to decreased amino acids compared to other tissues, the purpose of which is to break itself down to supply amino acids to other organs [22, 29]. This enhanced response is mediated through mTORC1 inactivation, as in other tissues, but also through a second much more potent muscle-specific pathway, FoxO3 [19]. This drastic macroautophagic response is highest in type II fast-twitch fibers [16, 22], which are the fibers with the highest degree of autophagic vacuolation and atrophy in XMEA [12, 36].

This work describes the clinical outcome at the cusp of tolerable reduction in V-ATPase. Beyond XMEA, it has implications for other, much more common, diseases. In malaria, the parasite inserts a V-ATPase into the erythrocyte membrane conferring itself optimal pH, and increased V-ATPase activity is an important component of HIV infection, osteoporosis, and cancer metastasis [8]. Our XMEA patients show that the safety margin of reducing V-ATPase activity in humans is wide, increasing the potential to utilize bafilomycin-related compounds, or RNAi against VMA21, as possible therapies against a host of diseases processes that rely on the V-ATPase.

Acknowledgments We wish to thank all the XMEA families. We are grateful to Drs. G. Israelian, V.C. Juel, M. Villanova, the late G. Karpati, S. Carpenter, and D. Figarella-Branger for the clinicopathologic diagnosis of some of the patients included in this study, previously published in clinical journals. We thank Drs. S. Grinstein for helpful discussions and Drs. J Rommens and S Meyn for their review of our manuscript, T. Sarkisyan, J. Kere, E. Heon, F. Zara and H. Lohi for ethnic control DNA samples, A. Leung for assistance with experiments in Supplemental Fig. 12, N. Ochtony for Supplemental Fig. 1A, P. Bradhsaw for assistance in deconvolution microscopy. Principal funding was from the Canadian Institutes of Health Research. The Association Française contre les Myopathies provided support to N. Levy, EVO Funds of Helsinki and Turku University Hospitals (Finland) and sports research grant from Ministry of Education of Finland to H. Kalimo, and the Natural Sciences and Engineering Research Council (Canada) to I. Munteanu.

Conflict of interest The authors declare that they have no conflicts of interests.

Ethical standard This study was approved by the Research Ethics Board of the Hospital for Sick Children Toronto and informed consent was obtained from all subjects.

References

1. Beugnet A, Tee AR, Taylor PM, Proud CG (2003) Regulation of targets of mTOR (mammalian target of rapamycin) signalling by intracellular amino acid availability. Biochem J 372:555–566
2. Blommaart EF, Luiken JJ, Blommaart PJ, van Woerkom GM, Meijer AJ (1995) Phosphorylation of ribosomal protein S6 is inhibitory for autophagy in isolated rat hepatocytes. J Biol Chem 270:2320–2326
3. Brummelkamp TR, Bernards R, Agami R (2002) A system for stable expression of short interfering RNAs in mammalian cells. Science 296:550–553
4. Cao Y, Klionsky DJ (2007) Physiological functions of Atg6/Beclin 1: a unique autophagy-related protein. Cell Res 17:839–849
5. Cuervo AM, Stefanis L, Fredenburg R, Lansbury PT, Sulzer D (2004) Impaired degradation of mutant alpha-synuclein by chaperone-mediated autophagy. Science 305:1292–1295
6. Demaurex N, Furuya W, D'Souza S, Bonifacino JS, Grinstein S (1998) Mechanism of acidification of the trans-Golgi network (TGN). In situ measurements of pH using retrieval of TGN38 and furin from the cell surface. J Biol Chem 273:2044–2051
7. Drose S, Altendorf K (1997) Bafilomycins and concanamycins as inhibitors of V-ATPases and P-ATPases. J Exp Biol 200:1–8
8. Forgac M (2007) Vacuolar ATPases: rotary proton pumps in physiology and pathophysiology. Nat Rev Mol Cell Biol 8: 917–929
9. Frattini A, Orchard PJ, Sobacchi C et al (2000) Defects in TCIRG1 subunit of the vacuolar proton pump are responsible for

a subset of human autosomal recessive osteopetrosis. Nat Genet 25:343–346
10. Fukuda K, Hirai Y, Yoshida H, Nakajima T, Usui T (1982) Free amino acid content of lymphocytes and granulocytes compared. Clin Chem 28:1758–1761
11. Huss M, Sasse F, Kunze B (2005) Archazolid and apicularen: novel specific V-ATPase inhibitors. BMC Biochem 6:13
12. Kalimo H, Savontaus ML, Lang H et al (1988) X-linked myopathy with excessive autophagy: a new hereditary muscle disease. Ann Neurol 23:258–265
13. Karet FE, Finberg KE, Nelson RD et al (1999) Mutations in the gene encoding B1 subunit of H^+-ATPase cause renal tubular acidosis with sensorineural deafness. Nat Genet 21:84–90
14. Kornak U, Reynders E, Dimopoulou A et al (2008) Impaired glycosylation and cutis laxa caused by mutations in the vesicular H^+-ATPase subunit ATP6V0A2. Nat Genet 40:32–34
15. Kovacs AL, Reith A, Seglen PO (1982) Accumulation of autophagosomes after inhibition of hepatocytic protein degradation by vinblastine, leupeptin or a lysosomotropic amine. Exp Cell Res 137:191–201
16. Li JB, Goldberg AL (1976) Effects of food deprivation on protein synthesis and degradation in rat skeletal muscles. Am J Physiol 231:441–448
17. Malicdan MC, Noguchi S, Nonaka I, Saftig P, Nishino I (2008) Lysosomal myopathies: an excessive build-up in autophagosomes is too much to handle. Neuromuscul Disord 18:521–529
18. Malkus P, Graham LA, Stevens TH, Schekman R (2004) Role of Vma21p in assembly and transport of the yeast vacuolar ATPase. Mol Biol Cell 15:5075–5091
19. Mammucari C, Schiaffino S, Sandri M (2008) Downstream of Akt: foxO3 and mTOR in the regulation of autophagy in skeletal muscle. Autophagy 4:524–526
20. Massey AC, Kaushik S, Sovak G, Kiffin R, Cuervo AM (2006) Consequences of the selective blockage of chaperone-mediated autophagy. Proc Natl Acad Sci USA 103:5805–5810
21. Mizushima N (2007) Autophagy: process and function. Genes Dev 21:2861–2873
22. Mizushima N, Yamamoto A, Matsui M, Yoshimori T, Ohsumi Y (2004) In vivo analysis of autophagy in response to nutrient starvation using transgenic mice expressing a fluorescent autophagosome marker. Mol Biol Cell 15:1101–1111
23. Munteanu I, Ramachandran N, Mnatzakanian GN et al (2008) Fine-mapping the gene for X-linked myopathy with excessive autophagy. Neurology 71:951–953
24. Nishino I, Fu J, Tanji K et al (2000) Primary LAMP-2 deficiency causes X-linked vacuolar cardiomyopathy and myopathy (Danon disease). Nature 406:906–910
25. Ostenfeld MS, Hoyer-Hansen M, Bastholm L et al (2008) Anticancer agent siramesine is a lysosomotropic detergent that induces cytoprotective autophagosome accumulation. Autophagy 4:487–499
26. Paroutis P, Touret N, Grinstein S (2004) The pH of the secretory pathway: measurement, determinants, and regulation. Physiology (Bethesda) 19:207–215
27. Salvador N, Aguado C, Horst M, Knecht E (2000) Import of a cytosolic protein into lysosomes by chaperone-mediated autophagy depends on its folding state. J Biol Chem 275: 27447–27456
28. Sandri M (2010) Autophagy in skeletal muscle. FEBS Lett 584:1411–1416
29. Scornik OA, Howell SK, Botbol V (1997) Protein depletion and replenishment in mice: different roles of muscle and liver. Am J Physiol 273:E1158–E1167
30. Scott JA, North ML, Rafii M et al (2011) Asymmetric dimethylarginine is increased in asthma. Am J Respir Crit Care Med 184:779–785
31. Shacka JJ, Klocke BJ, Shibata M et al (2006) Bafilomycin A1 inhibits chloroquine-induced death of cerebellar granule neurons. Mol Pharmacol 69:1125–1136
32. Sharma R, Deng H, Leung A, Mahuran D (2001) Identification of the 6-sulfate binding site unique to alpha-subunit-containing isozymes of human beta-hexosaminidase. Biochemistry 40:5440–5446
33. Stauber WT, Hedge AM, Trout JJ, Schottelius BA (1981) Inhibition of lysosomal function in red and white skeletal muscles by chloroquine. Exp Neurol 71:295–306
34. Tanaka Y, Guhde G, Suter A et al (2000) Accumulation of autophagic vacuoles and cardiomyopathy in LAMP-2-deficient mice. Nature 406:902–906
35. Taussky HH, Shorr E (1953) A microcolorimetric method for the determination of inorganic phosphorus. J Biol Chem 202: 675–685
36. Villanova M, Louboutin JP, Chateau D et al (1995) X-linked vacuolated myopathy: complement membrane attack complex on surface membrane of injured muscle fibers. Ann Neurol 37: 637–645
37. Webber JL, Tooze SA (2010) Coordinated regulation of autophagy by p38alpha MAPK through mAtg9 and p38IP. EMBO J 29:27–40
38. Zoncu R, Bar-Peled L, Efeyan A, Wang S, Sancak Y, Sabatini DM (2011) mTORC1 senses lysosomal amino acids through an inside-out mechanism that requires the vacuolar H(+)-ATPase. Science 334:678–683

ORIGINAL CONTRIBUTION

Myopathy Associated With Antibodies to Signal Recognition Particle

Disease Progression and Neurological Outcome

Shigeaki Suzuki, MD, PhD; Yukiko K. Hayashi, MD, PhD; Masataka Kuwana, MD, PhD; Rie Tsuburaya, MD, PhD; Norihiro Suzuki, MD, PhD; Ichizo Nishino, MD, PhD

Objective: To characterize the clinical course of myopathy associated with antibodies to signal recognition particle (SRP), or anti-SRP myopathy.

Design: Case series.

Setting: Keio University Hospitals and National Institute of Neuroscience, National Center of Neurology and Psychiatry, Tokyo, Japan.

Patients: We reviewed clinical features of 27 patients with anti-SRP myopathy and analyzed disease progression and neurological outcome.

Main Outcome Measures: Anti-SRP antibodies in serum were detected by RNA immunoprecipitation assay using extracts of K562 cells.

Results: Of the 27 patients, 5 (19%) showed chronic progressive muscle weakness as well as atrophy of limbs and trunk muscles from a younger age with more severe neurological outcomes compared with the other 22 patients (81%) with the subacute form.

Conclusion: A subset of patients with anti-SRP myopathy can show a chronic progressive form associated with severe clinical deficits.

Arch Neurol. 2012;69(6):728-732. Published online February 13, 2012. doi:10.1001/archneurol.2011.1728

Author Affiliations: Department of Neurology (Drs S. Suzuki and N. Suzuki) and Division of Rheumatology, Department of Internal Medicine (Dr Kuwana), Keio University School of Medicine, and Department of Neuromuscular Research, National Institute of Neuroscience, National Center of Neurology and Psychiatry (Drs Hayashi, Tsuburaya, and Nishino), Tokyo, Japan.

AUTOANTIBODIES AGAINST signal recognition particle (SRP) were first found in the serum of a patient with polymyositis and were listed as myositis-specific antibodies.[1] Myopathy associated with antibodies to SRP (anti-SRP myopathy) has recently been regarded as an immune-mediated necrotizing myopathy based on histological findings and has been clinically characterized by severe muscle weakness, marked elevation of serum creatine kinase (CK) levels, and poor response to corticosteroid therapy.[2-7] These observations were gathered mainly from patients with a clinical diagnosis of inflammatory myopathies. However, the clinical spectrum of anti-SRP myopathy may be broader.

The rapid progression of weakness is a characteristic clinical feature of anti-SRP myopathy.[2-7] The mean interval from its onset to diagnosis is 3 to 4 months, and clinical symptoms are usually progressive for 5 to 6 months.[3-5] In contrast, Dimitri et al[8] first described a 31-year-old man in whom weakness progressed for more than 3 years. Before the anti-SRP antibody was detected, he was diagnosed as having limb-girdle muscular atrophy. We also described a 32-year-old man with childhood-onset myopathy whose diagnosis alternated between inflammatory myopathy and muscular dystrophy for 21 years.[9] These results suggested that patients with anti-SRP myopathy can show chronic progression indistinguishable from muscular dystrophy. Herein, we analyzed the disease course and neurological outcomes in patients with anti-SRP myopathy.

METHODS

We chose 27 patients with myopathy with the anti-SRP antibody, including 10 previously reported cases.[9,10] The diagnosis of anti-SRP myopathy was based on clinical, electrophysiological, histopathological, and serological findings. Muscle weakness was assessed by manual muscle strength (Medical Research Council scale grade), and severe weakness was defined as grade 3 or lower. Muscle biopsy was performed in all 27 patients and showed fiber size variation as well as fiber necrosis and regeneration with or without lymphocyte infiltration. No patients had taken statins.

Anti-SRP antibodies were detected by RNA immunoprecipitation assay using extracts of K562 cells as previously described.[11] Briefly, 10 μL of serum was mixed with 2 mg of Protein A Sepharose CL-4B (Pharmacia Biotech AB) in 500 μL of immunoprecipitation buffer (10mM TRIS hydrochloride, pH 8.0, 500mM sodium chloride, 0.1% Nonidet P40) and incubated for 2 hours. After washing 3 times with immunoprecipitation buffer, antigen-bound Sepharose beads were mixed with 100 μL of K562 cell extract (6×10^6 cell equivalents per sample) for 2 hours, and 30 μL of 3M sodium acetate, 30 μL of 10% sodium dodecyl sulfate, and 300 μL of phenol:chloroform:isoamyl alcohol (50:50:1, containing 0.1% 8-hydroxyquinoline) were added to extract bound RNA. After ethanol precipitation, the RNA was resolved by using a 7M urea–8% polyacrylamide gel, and the gel was silver stained (Bio-Rad). Immunoprecipitated RNA located in the 7SL-RNA lesion was regarded as anti-SRP antibody. Other myositis-specific and myositis-associated autoantibodies were also detected by the RNA immunoprecipitation assay.

Neurological outcomes were assessed using the modified Rankin Scale (mRS).[12] This scale was principally used for evaluating function of patients with stroke; however, it was also applied to patients with myositis.[13] Neurological outcomes were divided into 3 groups: recovered, mild deficit, and severe deficit. Patients who responded optimally to the treatment and returned to their jobs (mRS score of 0-1) were defined as recovered. Patients who responded partially to treatment and resumed most activities of daily living (mRS score of 2-3) were defined as having a mild deficit. Patients who showed reworsening muscle weakness or re-elevation of serum CK levels after the treatment were also included in this group. Patients who responded minimally to the treatment and required support in daily activities (mRS score of 4) were defined as having a severe deficit.

This study was approved by the institutional review boards at Keio University and the National Center of Neurology and Psychiatry. Statistical analyses were performed using StatView version 5.0 statistical software (SAS Institute, Inc).

RESULTS

Figure 1 shows the distribution of periods between disease onset and the first examination. We divided 27 patients with anti-SRP myopathy into 2 subtypes (subacute and chronic forms) based on the clinical course. Of the 27 patients with anti-SRP myopathy in our study, 5 (19%) were considered to have the chronic form. The patients' demographic and clinical features are compared between those with the subacute and chronic forms (**Table 1**). Disease onset occurred at a younger age in those with the chronic form than in those with the subacute form (mean age, 15.4 vs 52.4 years, respectively; $P < .001$). No patients with the chronic form had a clear clinical history of antecedent infection, whereas 3 patients (14%) with the subacute form had antecedent infection. Despite a previous report,[5] seasonal occurrence was not clear in our series. Disease progression of the subacute form was usually rapid, and the mean duration between disease onset and the first examination was 3.1 months. In particular, 3 patients showed rapid disease progression in 2 to 3 weeks. In contrast, patients with the chronic form showed significantly slower progression, and the mean duration between disease onset and the first examination was 10.2 months ($P = .001$).

In our series, asymmetrical muscle involvement was seen in 2 patients, whereas the other 25 patients showed proximal-dominant symmetrical limb muscle weakness. Lower limbs were more severely affected than upper limbs. All 5 patients with the chronic form and about half of the patients with the subacute form showed severe muscle weakness and atrophy at the first examination. Several reports emphasized that dysphagia, but not dysarthria, was observed at a high frequency in 43% to 75% of patients with anti-SRP myopathy.[3,5,7] In our series, 7 patients (26%) had dysphagia and 3 (11%) reported it as the initial symptom. Previous reports also showed a high frequency of cardiac involvement,[2,5] while only 1 patient in our series had arrhythmias, which did not require treatment. Respiratory muscle involvement was detected in 3 patients. Myalgia was noted in 9 patients (36%) and tended to precede muscle weakness. Extramuscular manifestations were observed only in patients with the subacute form. Skin rash and interstitial lung disease, which were clinically suggestive of dermatomyositis, were observed in 2 and 4 patients, respectively. Serum CK levels were markedly elevated to more than 1000 IU/L (to convert to microkatals per liter, multiply by 0.0167) in all 27 patients; however, there was no difference between the subacute and chronic forms. Other autoantibodies were found in 6 patients with the subacute form, including Ro/SSA (3 patients), Th/To (1 patient), ribosome (1 patient), and U1RNP (1 patient).

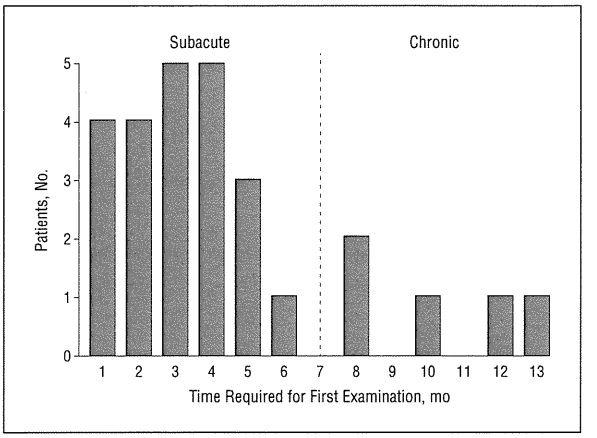

Figure 1. Period between disease onset and the first examination in 27 patients with anti–signal recognition particle myopathy. They were divided into 22 patients with the subacute form and 5 patients with the chronic form based on the clinical course.

All 27 patients were treated with oral prednisolone (1 mg/kg/d). Half of the patients were treated with additional immunosuppressive agents, including methotrexate (n = 5), azathioprine (n = 4), tacrolimus (n = 2), cyclophosphamide (n = 1), and cyclosporine (n = 1), or with intravenous immunoglobulin (n = 6). Although some patients required 2 to 3 months to respond to treatment, the patients with anti-SRP myopathy did not always respond poorly. The combination of oral prednisolone and intravenous immunoglobulin appears to be most effective for patients with the subacute form as the initial treatment. The neurological outcomes showed that 10 patients (45%) with the subacute form recovered. In contrast, all 5 patients with the chronic form had more severe neurological outcomes compared with the 22 patients with the subacute form ($P = .008$) (**Figure 2**).

Table 1. Comparison of Clinical Features Between Subacute and Chronic Forms of Anti–Signal Recognition Particle Myopathy

Clinical Feature	Patients, No. (%)		*P* Value
	Subacute (n = 22)	Chronic (n = 5)	
Age at onset, mean (range), y	52.4 (14-82)	15.4 (5-32)	<.001[a]
Female	12 (55)	3 (60)	.78[b]
Antecedent infection	3 (14)	0	.93[b]
Time required for first examination, mean (range), mo	3.1 (1-6)	10.2 (8-13)	.001[a]
Muscle weakness			
Arms < legs	16 (73)	3 (60)	.98[b]
Arms > legs	6 (27)	2 (40)	.98[b]
Severe involvement	11 (50)	5 (100)	.12[b]
Laterality	1 (5)	1 (20)	.80[b]
Facial muscle involvement	1 (5)	1 (20)	.80[b]
Bulbar sign	6 (27)	1 (20)	.81[b]
Cardiac involvement	1 (5)	0	.80[b]
Respiratory failure	3 (14)	1 (20)	.73[b]
Neck weakness	9 (41)	4 (80)	.27[b]
Muscle atrophy	10 (45)	5 (100)	.08[b]
Myalgia	8 (36)	1 (20)	.86[b]
Extramuscular involvement			
Fever	4 (18)	0	.73[b]
Skin rash	2 (9)	0	.80[b]
Arthritis	1 (5)	0	.80[b]
Raynaud phenomenon	1 (5)	0	.80[b]
Interstitial lung disease	4 (18)	0	.73[b]
Associated disorder			
Cancer	1 (9)	0	.80[b]
Rheumatic disorder	1 (9)	0	.80[b]
Serum creatine kinase, mean (range), IU/L	6101 (1149-15 585)	4190 (2465-5725)	.08[a]

SI conversion factor: To convert serum creatine kinase to microkatals per liter, multiply by 0.0167.
[a] Statistical analysis by *t* test.
[b] Statistical analysis by χ^2 test.

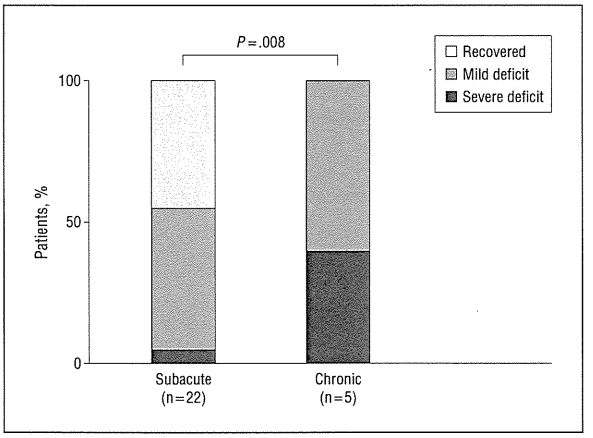

Figure 2. Neurological outcomes were assessed using the modified Rankin Scale[12] with some modifications and were compared between subacute and chronic forms of anti–signal recognition particle myopathy. The neurological outcomes were divided into recovered, mild deficit, and severe deficit. Differences between the groups were analyzed with the Mann-Whitney test. Five patients with the chronic form showed more severe outcomes than 22 patients with the subacute form (*P* = .008).

Detailed clinical features of 5 patients with the chronic form are summarized in **Table 2**. All patients had severe muscle weakness and marked atrophy in all 4 limbs and the trunk. Two patients (patients 2 and 5) noticed arm muscle weakness as the initial symptom. Importantly, scapular winging was noted in 2 patients (patients 2 and 3) at the first examination and was suspected to involve facioscapulohumeral muscular dystrophy. The serum CK level was decreased after treatment in patients with the chronic form, but muscle weakness gradually progressed and recovery of muscle strength was delayed. Three patients (patients 1, 2, and 3) became unable to walk independently, and 1 (patient 3) required mechanical ventilation. Because muscle biopsies were not suggestive of inflammatory myopathy, 1 patient (patient 3) was treated for only 3 months and 2 (patients 1 and 2) were treated after the detection of anti-SRP antibody. Of these younger patients, 2 (patients 2 and 3) became severely disabled, whereas the other 2 (patients 4 and 5) were treated soon after the muscle biopsy and responded partially to treatment.

COMMENT

There are 2 methods for detecting anti-SRP antibodies: the RNA immunoprecipitation assay we used and an immunoassay using the signal peptide–binding 54-kDa subunit of SRP (SRP54) as the antigen. Because SRP54 is regarded as the main antibody target, the immunoassay using SRP54 is easily conducted and the antibody level is also available.[1,2,14] However, epitopes of anti-SRP antibodies may also be located in other subunits of SRP proteins or 7SL-RNA.[7,15] In contrast, RNA immunoprecipitation assay, the standard method for detection of

Table 2. Clinical Features of 5 Patients With the Chronic Type of Anti–Signal Recognition Particle Myopathy

Feature	Patient No. 1[a]	2[a]	3[a]	4	5
Sex	F	F	M	F	M
Age at onset	5 y 9 mo	9 y 8 mo	10 y 2 mo	20 y 10 mo	32 y 9 mo
Initial symptoms	Frequent falls	Difficulty raising arm	Difficulty running fast	Difficulty climbing stairs	Difficulty raising his child
Weakness and atrophy	Proximal limbs (U < L); trunk	Proximal limbs (U > L); trunk; scapular winging; left dominant; myalgia	Proximal limbs (U < L); trunk; scapular winging; facial, bulbar; respiratory	Proximal limbs (U < L); trunk	Proximal limbs (U > L); trunk; strenocleidomastoideus
Serum creatine kinase, IU/L	4629	2467	4180	3951	5725
Muscle images	Atrophy in proximal limbs and trunk	Left-dominant atrophy and edematous change in proximal limbs and trunk	Atrophy and edematous change in proximal limbs and trunk	Atrophy and edematous change in proximal limbs and trunk	Atrophy and edematous change in proximal limbs and trunk
Age at muscle biopsy	6 y 5 mo	10 y 4 mo	11 y 3 mo, 16 y 6 mo	21 y 8 mo	33 y 9 mo
Muscle biopsy					
Variation in fiber size	Scattered	Scattered	Marked	Marked	Marked
Fiber necrosis and regeneration	Moderate	Marked	Marked	Scattered	Marked
Lymphocyte infiltration	None	None	None	None	Perivascular
Endomysial fibrosis	Minimal	Mild	Marked	Minimal	Mild
Age at anti-SRP antibody detection	7 y 4 mo	10 y 9 mo	32 y 6 mo	21 y 10 mo	34 y 3 mo
Age at treatment start	7 y 4 mo	10 y 9 mo	11 y 6 mo	21 y 8 mo	33 y 9 mo
Treatment	PSL, MTX, MPR	PSL, MTX, IVCY, AZA, tacrolimus	PSL (3 mo)	PSL, MPR	PSL, MTX, IVIg, tacrolimus
Age at final follow-up	9 y 3 mo	13 y 10 mo	34 y 8 mo	23 y 3 mo	35 y 6 mo
Response and neurological outcome	Partial response; progression for 2 y; relapse; MMT grade 4; Gowers sign	Minimal response; progression for 2 y; MMT grade 2-3; walking 20 m; difficulty in holding dishes	No response; progression for 3 y; recovered from mechanical ventilation; MMT grade 2-3; wheelchair use	Partial response; progression for 1 y; MMT grade 4	Partial response; progression for 1.5 y; weakness recovered; relapse

Abbreviations: AZA, azathioprine; IVCY, intravenous cyclophosphamide; IVIg, intravenous immunoglobulin; L, lower; MMT, manual muscle strength; MPR, high-dose methylprednisolone sodium succinate; MTX, methotrexate; PSL, prednisolone; SRP, signal recognition particle; U, upper.

SI conversion factor: To convert serum creatine kinase to microkatals per liter, multiply by 0.0167.

[a] These patients were previously described.[9,10]

anti-SRP antibodies, has advantages in sensitivity and specificity.[1,2,4,6,9,11] The RNA immunoprecipitation assay can recognize the conformational epitopes of SRP, although the titer of antibodies is not available. Many studies showed that anti-SRP antibodies were principally specific to myositis or necrotizing myopathy except in a few patients with systemic sclerosis or rheumatoid arthritis.[1,2,4,6,9,11] In regard to myopathies, we demonstrated that anti-SRP antibody was not detected in patients with various types of muscular dystrophy, and it was useful for the differential diagnosis of myopathies using RNA immunoprecipitation assay.[9]

Anti-SRP myopathy can show a wider variety of clinical symptoms than was previously considered. When weakness progresses rapidly, within 2 to 3 weeks, with extremely high serum CK levels (>10 000 IU/L), acute rhabdomyolysis should be differentiated.[8] When patients experience progressive weakness within 2 to 6 months[2-7] accompanied by interstitial lung disease, skin rash, or associated rheumatic disorders, polymyositis or dermatomyositis should be considered. Because skin rash is observed in approximately 10% of cases of anti-SRP myopathy in the present and previous studies,[5] anti-SRP antibodies may be also detected in patients clinically diagnosed as having dermatomyositis. In fact, Hamaguchi et al[16] reported that anti-SRP antibodies were detected in 7 of 376 patients (2%) with dermatomyositis using a similar detection method.

In our series, 5 of 27 patients with anti-SRP myopathy (19%) showed chronic progressive muscle involvement. The mean age at onset in these 5 patients was significantly younger than that of the patients with the subacute form, and patients with the chronic form showed severe weakness and atrophy in limbs and trunk muscles as well as poorer outcomes. It was speculated that the poor outcome may be partially ascribed to the delay of the first examination or anti-SRP antibodies detection. Importantly, these clinical features may indicate the possibility of muscular dystrophy rather than inflammatory myopathy,[8-10] although the disease progression was faster than occurs in muscular dystrophy. In fact, facioscapulohumeral muscular dystrophy was initially suspected in 2 patients owing to prominent shoulder-girdle weakness.[9,10]

It is well known that anti-SRP myopathy is usually resistant to treatment, resulting in severe disablement.[2-4,6,7] However, our observation suggested that patients with the subacute form had relatively good neurological outcomes. Early diagnosis by screening for anti-SRP antibodies is important for choosing intensive immunotherapy, which might contribute to better outcomes. In this regard, Hengstman et al[5] reported that the response to treatment for patients with anti-SRP myopathy did not differ significantly from that of myositis without anti-SRP antibodies. They reported that 75% of patients with anti-SRP myopathy could walk without any assistance after treatment. The severe outcomes of anti-SRP myopathy described in the previous studies may be attributable partly to results for patients with the chronic form. Rituximab therapy is potentially effective for patients with the chronic form.[7] Based on these findings, it may be useful to divide patients by disease progression to predict the neurological outcome.

An apparent question about the relationship between anti-SRP antibodies and muscle involvement is whether the anti-SRP antibodies themselves have any pathogenic effect against muscle. This hypothesis may be supported by several lines of data: (1) anti-SRP antibodies purified from patients' serum samples can inhibit the in vitro translocation of secretory proteins into endoplasmic reticulum[17]; (2) the levels of anti-SRP54 autoantibodies are closely associated with the levels of myolysis[14]; and (3) the removal of anti-SRP antibodies by plasma exchange improves muscle strength.[14,18] Nevertheless, the causal relationship between anti-SRP antibodies and muscle involvement is still not established, and further experiments such as passive transfer to animals are necessary to elucidate the pathogenesis of anti-SRP antibodies.

In conclusion, anti-SRP myopathy can show quite variable disease progression and neurological outcomes.

Accepted for Publication: August 23, 2011.
Published Online: February 13, 2012. doi:10.1001/archneurol.2011.1728
Correspondence: Shigeaki Suzuki, MD, PhD, Department of Neurology, Keio University School of Medicine, 35 Shinanomachi, Shinjuku-ku, Tokyo 160-8582, Japan (sgsuzuki@z3.keio.jp).
Author Contributions: Dr S. Suzuki had full access to all of the data in the study and takes responsibility for the integrity of the data and the accuracy of the data analysis. *Study concept and design:* S. Suzuki, Hayashi, and Nishino. *Acquisition of data:* S. Suzuki and Tsuburaya. *Analysis and interpretation of data:* S. Suzuki, Hayashi, Kuwana, and N. Suzuki. *Drafting of the manuscript:* S. Suzuki and Hayashi. *Critical revision of the manuscript for important intellectual content:* Kuwana, Tsuburaya, N. Suzuki, and Nishino. *Statistical analysis:* S. Suzuki. *Obtained funding:* S. Suzuki, Hayashi, and Nishino. *Administrative, technical, and material support:* Hayashi, Kuwana, Tsuburaya, and N. Suzuki. *Study supervision:* Nishino.
Financial Disclosure: None reported.

Funding/Support: This work was supported by grant 18790601 from the Japanese Ministry of Education, Science, Sports, and Culture, by a Neuroimmunological Disease Research Committee grant from the Japanese Ministry of Health, Labour, and Welfare, by a Grant-in-Aid for Scientific Research from the Japan Society for the Promotion of Science, by Health Labour Sciences Research Grant 20B-12, 20B-13 for Research on Psychiatric and Neurological Diseases and Mental Health, Research on Measures for Intractable Diseases, and Research on Nervous and Mental Disorders from the Ministry of Health, Labor, and Welfare, and by Intramural Research Grant 23-4, 23-5, 23-6 for Neurological and Psychiatric Disorders at the National Center of Neurology and Psychiatry.

REFERENCES

1. Reeves WH, Nigam SK, Blobel G. Human autoantibodies reactive with the signal-recognition particle. *Proc Natl Acad Sci U S A.* 1986;83(24):9507-9511.
2. Targoff IN, Johnson AE, Miller FW. Antibody to signal recognition particle in polymyositis. *Arthritis Rheum.* 1990;33(9):1361-1370.
3. Miller T, Al-Lozi MT, Lopate G, Pestronk A. Myopathy with antibodies to the signal recognition particle: clinical and pathological features. *J Neurol Neurosurg Psychiatry.* 2002;73(4):420-428.
4. Kao AH, Lacomis D, Lucas M, Fertig N, Oddis CV. Anti-signal recognition particle autoantibody in patients with and patients without idiopathic inflammatory myopathy. *Arthritis Rheum.* 2004;50(1):209-215.
5. Hengstman GJ, ter Laak HJ, Vree Egberts WT, et al. Anti-signal recognition particle autoantibodies: marker of a necrotising myopathy. *Ann Rheum Dis.* 2006;65(12):1635-1638.
6. Takada T, Hirakata M, Suwa A, et al. Clinical and histopathological features of myopathies in Japanese patients with anti-SRP autoantibodies. *Mod Rheumatol.* 2009;19(2):156-164.
7. Valiyil R, Casciola-Rosen L, Hong G, Mammen A, Christopher-Stine L. Rituximab therapy for myopathy associated with anti-signal recognition particle antibodies: a case series. *Arthritis Care Res (Hoboken).* 2010;62(9):1328-1334.
8. Dimitri D, Andre C, Roucoules J, Hosseini H, Humbel RL, Authier FJ. Myopathy associated with anti-signal recognition peptide antibodies: clinical heterogeneity contrasts with stereotyped histopathology. *Muscle Nerve.* 2007;35(3):389-395.
9. Suzuki S, Satoh T, Sato S, et al. Clinical utility of anti-signal recognition particle antibody in the differential diagnosis of myopathies. *Rheumatology (Oxford).* 2008;47(10):1539-1542.
10. Suzuki S, Ohta M, Shimizu Y, Hayashi YK, Nishino I. Anti-signal recognition particle myopathy in the first decade of life. *Pediatr Neurol.* 2011;45(2):114-116.
11. Okada N, Mimori T, Mukai R, Kashiwagi H, Hardin JA. Characterization of human autoantibodies that selectively precipitate the 7SL RNA component of the signal recognition particle. *J Immunol.* 1987;138(10):3219-3223.
12. van Swieten JC, Koudstaal PJ, Visser MC, Schouten HJ, van Gijn J. Interobserver agreement for the assessment of handicap in stroke patients. *Stroke.* 1988;19(5):604-607.
13. Danieli MG, Calcabrini L, Calabrese V, Marchetti A, Logullo F, Gabrielli A. Intravenous immunoglobulin as add on treatment with mycophenolate mofetil in severe myositis. *Autoimmun Rev.* 2009;9(2):124-127.
14. Benveniste O, Drouot L, Jouen F, et al. Correlation of anti-signal recognition particle autoantibody levels with creatine kinase activity in patients with necrotizing myopathy. *Arthritis Rheum.* 2011;63(7):1961-1971.
15. Satoh T, Okano T, Matsui T, et al. Novel autoantibodies against 7SL RNA in patients with polymyositis/dermatomyositis. *J Rheumatol.* 2005;32(9):1727-1733.
16. Hamaguchi Y, Kuwana M, Hoshino K, et al. Clinical correlations with dermatomyositis-specific autoantibodies in adult Japanese patients with dermatomyositis: a multicenter cross-sectional study. *Arch Dermatol.* 2011;147(4):391-398.
17. Römisch K, Miller FW, Dobberstein B, High S. Human autoantibodies against the 54 kDa protein of the signal recognition particle block function at multiple stages. *Arthritis Res Ther.* 2006;8(2):R39.
18. Arlet JB, Dimitri D, Pagnoux C, et al. Marked efficacy of a therapeutic strategy associating prednisone and plasma exchange followed by rituximab in two patients with refractory myopathy associated with antibodies to the signal recognition particle (SRP). *Neuromuscul Disord.* 2006;16(5):334-336.

ARTICLE IN PRESS
MATBIO-00900; No of Pages 12
Matrix Biology xxx (2012) xxx–xxx
Contents lists available at SciVerse ScienceDirect
Matrix Biology
journal homepage: www.elsevier.com/locate/matbio

Perlecan modulates VEGF signaling and is essential for vascularization in endochondral bone formation

Muneaki Ishijima [a,b], Nobuharu Suzuki [a], Kentaro Hozumi [a], Tomoya Matsunobu [a], Keisuke Kosaki [a], Haruka Kaneko [b], John R. Hassell [c], Eri Arikawa-Hirasawa [d], Yoshihiko Yamada [a,*]

[a] Laboratory of Cell and Developmental Biology, National Institute of Dental and Craniofacial Research, National Institutes of Health, Bethesda, Maryland 20892-4370, USA
[b] Department of Medicine for Motor Organs, Juntendo University Graduate School of Medicine, Tokyo 113-8421, Japan
[c] Department of Molecular Medicine, College of Medicine, University of South Florida, Tampa, FL 33612-4799, USA
[d] Research Institute for Diseases of Old Age, Juntendo University Graduate School of Medicine, Tokyo 113-8421, Japan

ARTICLE INFO

Article history:
Received 30 November 2011
Received in revised form 27 February 2012
Accepted 28 February 2012
Available online xxxx

Keywords:
Perlecan
Endochondral bone formation
Growth plate
Vascular invasion
VEGF signaling

ABSTRACT

Perlecan (Hspg2) is a heparan sulfate proteoglycan expressed in basement membranes and cartilage. Perlecan deficiency ($Hspg2^{-/-}$) in mice and humans causes lethal chondrodysplasia, which indicates that perlecan is essential for cartilage development. However, the function of perlecan in endochondral ossification is not clear. Here, we report the critical role of perlecan in VEGF signaling and angiogenesis in growth plate formation. The $Hspg2^{-/-}$ growth plate was significantly wider but shorter due to severely impaired endochondral bone formation. Hypertrophic chondrocytes were differentiated in $Hspg2^{-/-}$ growth plates; however, removal of the hypertrophic matrix and calcified cartilage was inhibited. Although the expression of MMP-13, CTGF, and VEGFA was significantly upregulated in $Hspg2^{-/-}$ growth plates, vascular invasion into the hypertrophic zone was impaired, which resulted in an almost complete lack of bone marrow and trabecular bone. We demonstrated that cartilage perlecan promoted activation of VEGF/VEGFR by binding to the VEGFR of endothelial cells. Expression of the perlecan transgene specific to the cartilage of $Hspg2^{-/-}$ mice rescued their perinatal lethality and growth plate abnormalities, and vascularization into the growth plate was restored, indicating that perlecan in the growth plate, not in endothelial cells, is critical in this process. These results suggest that perlecan in cartilage is required for activating VEGFR signaling of endothelial cells for vascular invasion and for osteoblast migration into the growth plate. Thus, perlecan in cartilage plays a critical role in endochondral bone formation by promoting angiogenesis essential for cartilage matrix remodeling and subsequent endochondral bone formation.

Published by Elsevier B.V.

1. Introduction

Most bones, such as the long bones, are formed by endochondral ossification, in which cartilage during growth is first formed as a template and then replaced by bone (Karsenty, 2003; Kronenberg, 2003). Endochondral ossification is initiated by the condensation of mesenchymal cells, which differentiate into chondrocytes. The cells surrounding the mesenchyme condensation differentiate into the perichondrium. Proliferating chondrocytes produce a large number of matrix molecules, such as collagen II and aggrecan, to expand the cartilage template, cease proliferation at the prehypertrophic zone in the middle of the growth plate, and further differentiate into collagen X-expressing hypertrophic chondrocytes. The matrix surrounding mature hypertrophic chondrocytes is mineralized and replaced with osteoblasts. Although cartilage is a neovascular tissue, factors such as vascular endothelial growth factor (VEGF) produced by hypertrophic chondrocytes induce vascular invasion into the perichondrium and cartilage near the terminal region of the cartilage template, which is required for cartilage matrix remodeling and osteoblast migration from the perichondrium for ossification and bone marrow formation (Zelzer et al., 2004). This indicates that endochondral bone formation is a process highly coordinated between chondrogenesis and osteogenesis.

Perlecan plays critical roles in normal development, tissue functions, and diseases (Olsen, 1999; DeCarlo and Whitelock, 2006; Knox and Whitelock, 2006; Zoeller et al., 2009). Perlecan is a proteoglycan present in all basement membranes and other tissues, such as cartilage, plays important roles in development and tissue functions, and is associated with various diseases (Olsen, 1999; Morita et al., 2005; DeCarlo and Whitelock, 2006; Knox and Whitelock, 2006; Zoeller et al., 2009). Perlecan consists of a large elongated core protein with a complex modular structure and is usually substituted with several heparan sulfate and/or chondroitin sulfate chains (Noonan et al.,

* Corresponding author at: Bldg. 30, Rm. 407, NIDCR, NIH, 30 Convent Drive MSC 4370, Bethesda, MD 20892-4370, USA. Tel.: +1 301 496 2111; fax: +1 301 402 0897.
E-mail address: yoshi.yamada@nih.gov (Y. Yamada).

0945-053X/$ – see front matter. Published by Elsevier B.V.
doi:10.1016/j.matbio.2012.02.006

Please cite this article as: Ishijima, M., et al., Perlecan modulates VEGF signaling and is essential for vascularization in endochondral bone formation, Matrix Biology (2012), doi:10.1016/j.matbio.2012.02.006

1991). Perlecan binds basement membrane components, such as laminins and collagen IV, providing scaffolding for cells in many tissues and creating a barrier to the passage of molecules in the kidneys (Hopf et al., 1999; Morita et al., 2005). Perlecan also binds other extracellular proteins, such as fibronectin and fibulin. Perlecan modulates cell proliferation and differentiation through interaction with cell surface receptors such as integrins and with growth factors such as FGFs (Aviezer et al., 1994; Brown et al., 1997). Many biological functions of perlecan have been reported, such as aiding supramolecular organization of basement membranes and cell-matrix interactions (Brown et al., 1997; Hopf et al., 1999; Kvist et al., 2006), storage and release of various cytokines (Klein et al., 1995; Whitelock et al., 1996; Ghiselli et al., 2001; Govindraj et al., 2006; Smith et al., 2007), control of extracellular proteolysis and macromolecular filtration (Mongiat et al., 2003; Morita et al., 2005), and angiogenesis (Aviezer et al., 1994; Jiang and Couchman, 2003; Segev et al., 2004; Zhou et al., 2004).

Studies in knockout mice and mutations in the perlecan gene (HSPG2) in humans revealed that perlecan is essential for cartilage development (Arikawa-Hirasawa et al., 1999; Costell et al., 1999; Arikawa-Hirasawa et al., 2001a,b). Perlecan knockout ($Hspg2^{-/-}$) mice develop severe skeletal dysplasia characterized by shortened bones and craniofacial abnormalities and die shortly after birth of respiratory failure due to the cartilage defects of the rib cage (Arikawa-Hirasawa et al., 1999; Costell et al., 1999). Proliferation of chondrocytes is reduced in $Hspg2^{-/-}$ mice (Arikawa-Hirasawa et al., 1999). The cartilage matrix of the knockout mice contains disorganized collagen fibrils and glycosaminoglycans, which suggests that perlecan plays an important role in the cartilage matrix structure (Kvist et al., 2006). A human disorder, dyssegmental dysplasia, Silverman-Handmaker type (DDSH), was identified as a functional null mutation of perlecan and causes skeletal abnormalities similar to those of the knockout mice (Arikawa-Hirasawa et al., 2001a,b). In addition, subtle functional mutations of perlecan cause Schwartz-Jampel Syndrome (SJS), a rare autosomal recessive osteochondrodysplasia associated with myotonia (Nicole et al., 2000; Arikawa-Hirasawa et al., 2002; Rodgers et al., 2007). Patients with SJS survive and show much milder skeletal dysplasia compared to those with DDSH. We also showed that perlecan is critical for maintaining fast muscle mass and fiber composition by regulating myostatin signaling

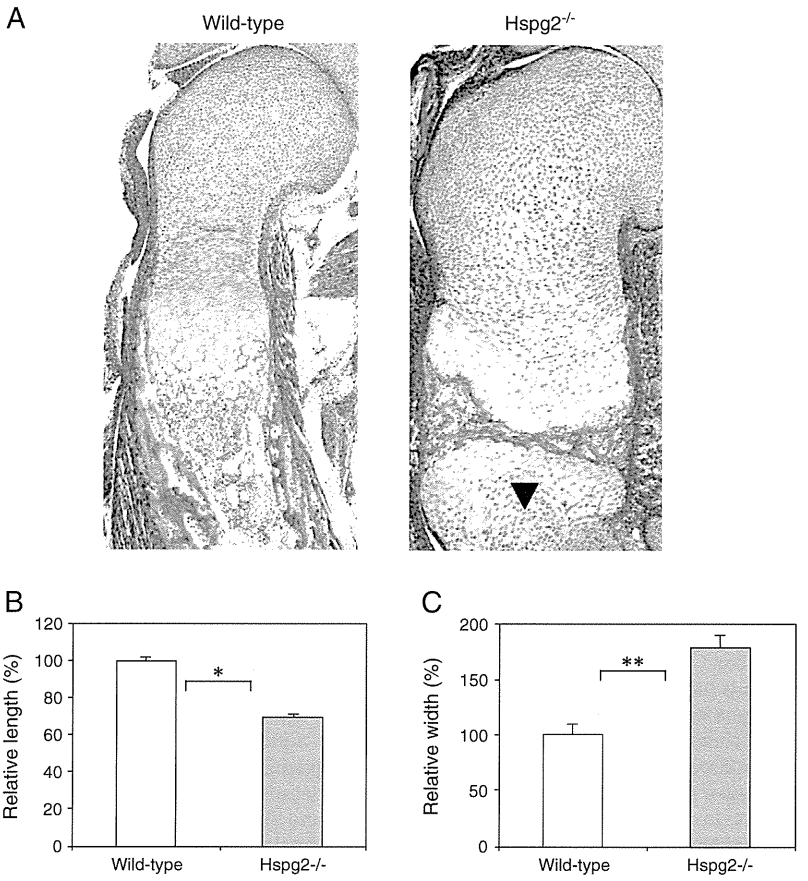

Fig. 1. Endochondral ossification was impaired in the growth plate of $Hspg2^{-/-}$ mice. (A) H-E staining of the proximal end of the humerus in E16.5 wild-type and $Hspg2^{-/-}$ mice. The long bones of $Hspg2^{-/-}$ mice were shorter than those of wild-type mice, as the distal end of the growth plate (arrowhead) was observed in $Hspg2^{-/-}$ mice but not in wild-type mice. (B) Comparison of the humeral length of $Hspg2^{-/-}$ mice with that of wild-type mice. The relative length of the humerus in wild-type mice was set at 100%. * indicates $p<0.05$. **(C)** Comparison of the humeral width of $Hspg2^{-/-}$ mice with that of wild-type. The relative width of the humerus in wild-type mice was set at 100%. **Indicates $p<0.01$. **(D)** Double staining of Safranin-O (red) and von Kossa (brown) staining of the proximal end of the humerus at E16.5 in wild-type and $Hspg2^{-/-}$ mice. Reduced glycosaminoglycan levels in the growth plate of $Hspg2^{-/-}$ mice were observed compared with those of wild-type mice. In the growth plates of wild-type mice, the terminal hypertrophic zone was replaced with trabecular bone, and the perichondrium formed bone collars by membranous ossification. The bone collar aligns parallel to the longitudinal axis of the limb. In $Hspg2^{-/-}$ mice, levels of the calcified matrix in the terminal cartilage template were increased, and levels in the trabecular bone were reduced. Boxed areas are enlarged and shown below. (For interpretation of the references to color in this figure legend, the reader is referred to the web version of this article.)

Please cite this article as: Ishijima, M., et al., Perlecan modulates VEGF signaling and is essential for vascularization in endochondral bone formation, Matrix Biology (2012), doi:10.1016/j.matbio.2012.02.006

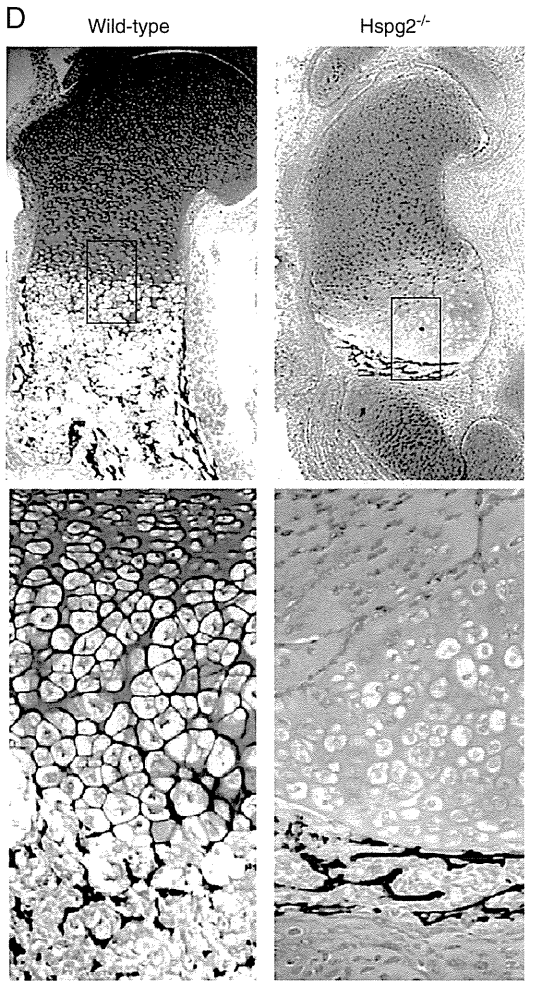

Fig. 1 (*continued*).

using lethality-rescued Hspg2$^{-/-}$-Tg mice by expressing recombinant perlecan specifically in the cartilage of the perlecan-null (Hspg2$^{-/-}$) genetic background (Xu et al., 2010), where perlecan is expressed in cartilage but absent in muscle, endothelial basement membranes, and other tissues.

Although perlecan plays a critical role in growth plate development, the function of perlecan in endochondral ossification is not clear. Here we analyzed the growth plates of Hspg2$^{-/-}$ and Hspg2$^{-/-}$-Tg mice and demonstrated that perlecan in cartilage, not in endothelial basement membranes, is required for vascular invasion and cartilage matrix remodeling that is essential for the formation of the trabecular bone and bone marrow.

2. Results

2.1. Endochondral ossification is inhibited in the growth plate of Hspg2$^{-/-}$ mice

Perlecan is essential for cartilage development, as perlecan deficiency in mice displays perinatal lethal chondrodysplasia (Arikawa-Hirasawa et al., 1999; Costell et al., 1999). In humans, null mutations of perlecan cause severe chondrodysplasia and DDSH, similar to Hspg2$^{-/-}$ mice. The humeri of E16.5 Hspg2$^{-/-}$ mice were shorter and wider than those of wild-type mice (Fig. 1A). Quantification analyses revealed that the humeri of Hspg2$^{-/-}$ mice were significantly shorter (Fig. 1B) and wider (Fig. 1C) compared to those of wild-type mice. The humeri of Hspg2$^{-/-}$ mice contained reduced levels of glycosaminoglycan, as shown with Safranin-O staining (Fig. 1D, red) and as described previously (Arikawa-Hirasawa et al., 1999; Costell et al., 1999). The striking abnormality of the growth plate of mutant mice is the almost complete lack of bone marrow cavities and trabecular bone (Fig. 1). In the E16.5 growth plates of wild-type mice, von Kossa staining (brown) showed that bone collar and trabecular bone were formed, and calcification of the matrix surrounding mature hypertrophic chondrocytes, as well as of the matrix surrounding the periosteum (bone collar) and trabecular bone, was observed (Fig. 1D). In contrast, in Hspg2$^{-/-}$ mice, thin calcified layers were observed along the bottom border of the cartilage and separated two cartilage regions, which were located close together in the almost complete absence of bone marrow.

2.2. Defect of perlecan in chondrocytes inhibits vascular invasion into the hypertrophic chondrocyte

The inhibition of the formation of bone marrow and trabecular bone suggests a defect in angiogenesis in the hypertrophic zone in Hspg2$^{-/-}$ growth plates. Therefore, we examined vascular invasion into the hypertrophic zone. Immunostaining of CD31 (PCAM-1), a marker of endothelial cells, showed that endothelial cells invaded cartilage from surrounding tissues, including the perichondrium and bone marrow, in wild-type mice (Fig. 2A). The chondro-osseous region was arranged perpendicularly to the long axis of the bone (Fig. 2A) in wild-type mice. In Hspg2$^{-/-}$ mice, bone marrow was almost completely absent, and CD31-positive endothelial cells (black) were observed in the perichondrium/periosteum and surrounding tissues (Fig. 2A). In addition, the proximal and distal cartilage areas were separated by thin calcified layers in the humeri of the Hspg2$^{-/-}$ mice (Figs. 1A, B, and 2A). These results suggest that vascular invasion into the hypertrophic zone from the surrounding tissues was severely inhibited in the absence of perlecan. TRAP-positive osteoclasts with multiple nuclei, which are differentiated from hematopoietic stem cells, migrated into the cartilage-bone interface and trabecular bone through the vasculature in wild-type mice (Fig. 2B). TRAP-positive osteoclasts (dark red) were present, but their numbers were reduced in the bone collar and surrounding region of the Hspg2$^{-/-}$ growth plates (Fig. 2B). These results further indicate that vascular invasion into the growth plate is impaired in Hspg2$^{-/-}$ mice.

2.3. VEGFA expression is increased in chondrocytes of Hspg2$^{-/-}$ mice

Vascular invasion is a crucial step in removing the cartilage matrix for endochondral ossification. VEGFA plays an important role in vascular invasion for endochondral ossification (Maes et al., 2002; Zelzer et al., 2002; Maes et al., 2004; Zelzer et al., 2004). Therefore, we examined the VEGFA protein expression level in chondrocytes in HSPG2$^{-/-}$ mice with immunostaining and confirmed with Western blot (Fig. 3). In Hspg2$^{-/-}$ mice, the expression levels of VEGFA proteins in hypertrophic chondrocytes were substantially increased compared with the control mice (Fig. 3A). Consistent with this immunostaining result, Western blotting revealed that VEGFA protein levels in the Hspg2$^{-/-}$ growth plate were increased compared to those in the wild-type growth plate (Fig. 3B).

2.4. VEGF$_{164}$ expression is increased in chondrocytes of Hspg2$^{-/-}$ mice

VEGFA consists of three splice variants, VEGF$_{120}$, VEGF$_{164}$, and VEGF$_{188}$ (Ruhrberg et al., 2002). Although VEGF$_{120}$, which does not have a heparan sulfate binding site in the C-terminal region, is important for vascular invasion in the epiphysis of the growth plate to form

Please cite this article as: Ishijima, M., et al., Perlecan modulates VEGF signaling and is essential for vascularization in endochondral bone formation, Matrix Biology (2012), doi:10.1016/j.matbio.2012.02.006

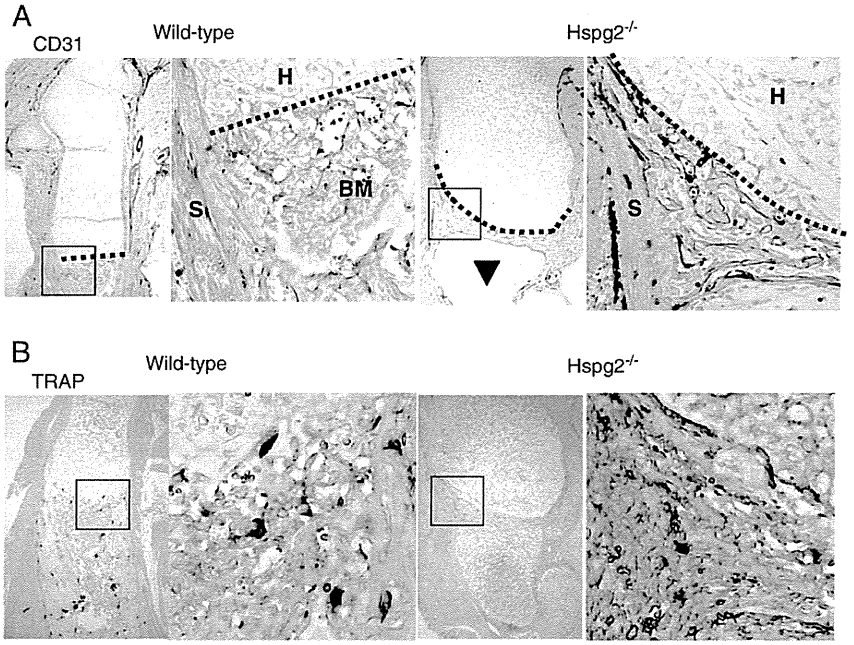

Fig. 2. Vascular invasion into the hypertrophic zone is inhibited in Hspg2$^{-/-}$ mice. (A) Immunostaining of CD31 (PCAM-1) (black) shows that endothelial cells invaded the chondro-osseous boundary and bone marrow from surrounding tissues in wild-type mice. Dotted line, chondro-osseous boundary; bone marrow (BM); hypertrophic zone (H); surrounding tissues (S). The dotted line in the growth plates of Hspg2$^{-/-}$ mice indicates the boundary between the hypertrophic zone and the abnormally curved perichondrium layer and bone collar surrounding the terminal hypertrophic zone. (B) Osteoclast differentiation was inhibited in the growth plates of Hspg2$^{-/-}$ mice. Multinucleated TRAP-positive osteoclasts (dark red) were observed in the chondro-osseous boundary as well as bone marrow in wild-type mice. In Hspg2$^{-/-}$ mice, TRAP-positive osteoclast numbers are lower in the boundary. (For interpretation of the references to color in this figure legend, the reader is referred to the web version of this article.)

the secondary ossification center (Maes et al., 2004), $VEGF_{164}$, which contains one of the two heparan sulfate binding sites, is critical for vascular invasion to form trabecular bone in the growth plate (Zelzer et al., 2004). We examined the mRNA expression levels of these isoforms of VEGFA in the growth plate chondrocytes in Hspg2$^{-/-}$ mice. Although two VEGF mRNA isoforms were expressed in chondrocytes prepared from the growth plates of wild-type mice, the expression levels of $VEGF_{164}$ were more dominant than those of $VEGF_{120}$ (Fig. 4A). In Hspg2$^{-/-}$ mice, these VEGF mRNA were also expressed, but their expression levels were found to be increased further than those in wild-type mice by using semi-quantitative RT-PCR analysis (Fig. 4A). Real-time PCR analysis of the expression levels of these three isoforms showed that, although these isoforms of VEGF mRNA were significantly increased in chondrocytes of Hspg2$^{-/-}$ mice compared to those of wild-type mice, the $VEGF_{164}$ mRNA levels were most profoundly increased in the absence of perlecan (Fig. 4B). These results indicate that the VEGFA expression level was not a major cause of the defect in vascular invasion into the growth plate cartilage of Hspg2$^{-/-}$ mice.

2.5. Expression of CTGF, Chm-1, and MMPs in the hypertrophic chondrocytes of Hspg2$^{-/-}$ mice

In addition to VEGFA, connective tissue growth factor (CTGF) plays an important role in vascular invasion in endochondral ossification. The absence of CTGF impairs vascular invasion (Ivkovic et al., 2003), while the absence of chondromodulin-1 (Ch-1) in vivo does not impair vascular invasion (Brandau et al., 2002). We found that the CTGF and Ch-1 mRNA levels in Hspg2$^{-/-}$ mice were significantly increased compared with those of the wild-type mice (Fig. 5A, B). Matrix metalloproteinases (MMPs) are also important for vascular invasion, as MMPs degrade most components of the extracellular matrix (ECM) that allow promotion of sprouting and migration of endothelial cells (Noel et al., 2004; Sottile, 2004). We found that the MMP13 mRNA levels were significantly increased in the growth plates of Hspg2$^{-/-}$ mice compared with those of wild-type mice (Fig. 5C). MMP-9 is also expressed in the hypertrophic chondrocytes of wild-type mice and Hspg2$^{-/-}$ mice (data not shown)(Gustafsson et al., 2003). These results indicate that the inhibition of vascular invasion in the growth plates of Hspg2$^{-/-}$ mice was not due to the reduced expression levels of CTGF and MMP.

2.6. Removal of hypertrophic matrix is inhibited in the absence of perlecan

We examined cartilage calcification and osteopontin (OPN) expression in E18.5 Hspg2$^{-/-}$ growth plates. Type X collagen expression was observed in Hspg2$^{-/-}$ mice (data not shown), as reported previously, although its expression levels are decreased in Hspg2$^{-/-}$ mice compared with those in wild-type mice (Arikawa-Hirasawa et al., 1999; Costell et al., 1999). At E18.5, formation of hydroxyapatite nodules (calcospherites) was observed in the hypertrophic zone of Hspg2$^{-/-}$ mice, which is one of the characteristics of the defects in perlecan-deficient cartilage in mice and humans (Arikawa-Hirasawa et al., 1999)(Fig. 6A). In addition, although the calcified matrix was observed only in the last few layers of hypertrophic chondrocytes in wild-type mice, the calcified matrix was found in multiple layers in the hypertrophic zone in perlecan-deficient mice, suggesting impaired remodeling of the calcified cartilage matrix. The expression of OPN mRNA, a marker of terminally differentiated mature chondrocytes, was significantly increased in chondrocytes in Hspg2$^{-/-}$ mice compared with those in wild-type mice (Fig. 6B). In wild-type growth plates, perlecan (red) was expressed and surrounded hypertrophic

Please cite this article as: Ishijima, M., et al., Perlecan modulates VEGF signaling and is essential for vascularization in endochondral bone formation, Matrix Biology (2012), doi:10.1016/j.matbio.2012.02.006

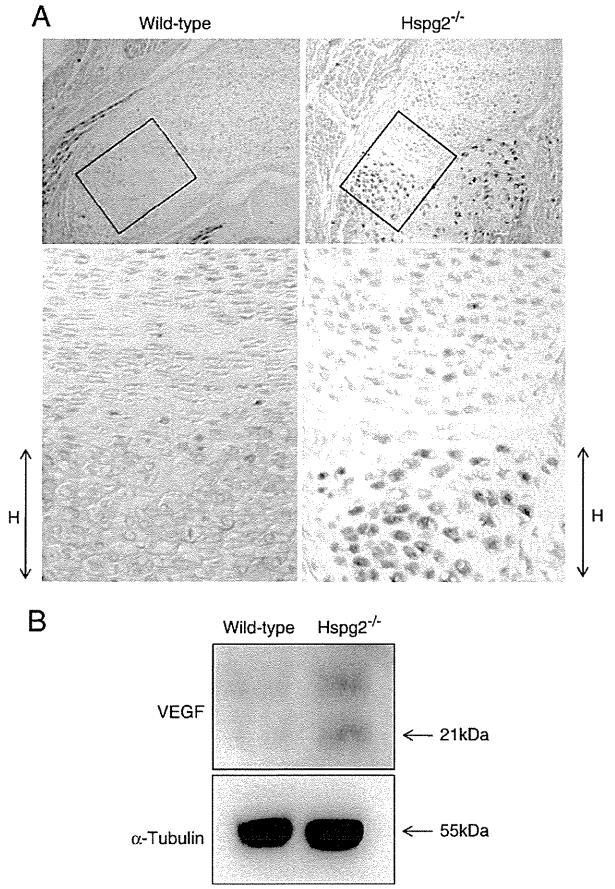

Fig. 3. Increased VEGF expression by chondrocytes in Hspg2$^{-/-}$ mice. (A) Immunostaining of VEGFA. Expression of VEGFA in prehypertrophic and hypertrophic chondrocytes was increased in Hspg2$^{-/-}$ mice compared to that in wild-type mice. Hypertrophic zone (H). (B) Western blot of VEGFA protein. The expression level of the VEGFA proteins was increased further in the chondrocytes of Hspg2$^{-/-}$ mice compared to that in wild-type mice.

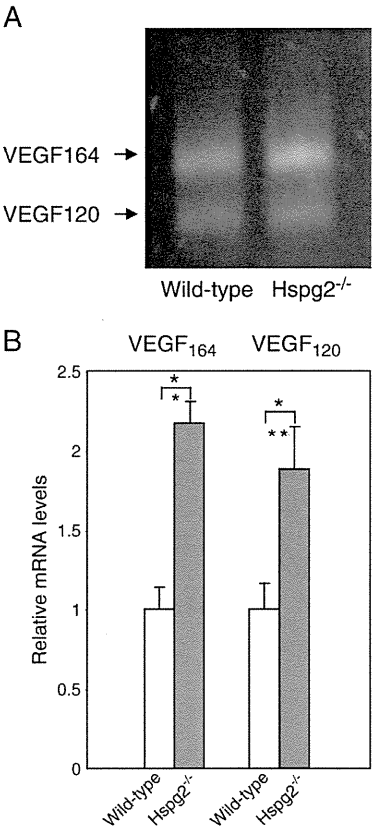

Fig. 4. $VEGF_{164}$ expression is increased in chondrocytes of Hspg2$^{-/-}$ mice. (A) Semi-quantitative RT-PCR of VEGF isoforms. $VEGF_{120}$ and $VEGF_{164}$ mRNA were expressed in chondrocytes prepared from the growth plates of wild-type mice. Expression levels of $VEGF_{164}$ mRNA were most prominent in wild-type mice. In Hspg2$^{-/-}$ mice, these VEGF mRNA were also expressed, with the highest level for $VEGF_{164}$. (B) Real-time RT-PCR analysis of the expression levels of VEGF mRNA in chondrocytes in wild-type and Hspg2$^{-/-}$ mice. $VEGF_{120}$ and $VEGF_{164}$ mRNA were increased in the chondrocytes of Hspg2$^{-/-}$ mice. The increase in the levels of $VEGF_{164}$ mRNA was largest in the absence of perlecan. The relative expression levels of each isoform in wild-type mice were set as 1. *Indicates $p<0.05$.

chondrocytes, while perlecan was absent in Hspg2$^{-/-}$ mice (Fig. 6C) (Xu et al., 2010).

Immunohistochemical analyses revealed that the OPN protein (green) was expressed at the end layer of hypertrophic chondrocytes in wild-type mice. However, in Hspg2$^{-/-}$ growth plates, OPN protein expression was observed in multiple layers of hypertrophic chondrocytes (Fig. 6C). These results suggest that remodeling of the hypertrophic matrix was inhibited in Hspg2$^{-/-}$ mice.

2.7. Inhibition of vascular invasion is due to the defect of perlecan in chondrocytes, but not in endothelial cells

Perlecan is expressed not only in chondrocytes but also in all basement membranes, including vessel walls. Therefore, the inhibition of vascular invasion in the hypertrophic zone in the absence of perlecan could have been due to the absence of perlecan in the basement membranes of endothelial cells. To exclude this possibility, mice in which perlecan was expressed specifically in chondrocytes were created by introducing the transgene (Per-Tg) under the control of a cartilage-specific Col2a1 promoter and enhancer in the Hspg2$^{-/-}$ genetic background (Hspg2$^{-/-}$-Tg mice) (Xu et al., 2010). In the Hspg2$^{-/-}$-Tg mice, perlecan is expressed in cartilage but absent in the basement membranes of blood vessels, muscle, and other tissues surrounding cartilage (Xu et al., 2010). The bone sizes of the HSPG2$^{-/-}$-Tg mice were similar to those of wild-type mice (Fig. 7A). Histological analysis showed that the columnar structure of the growth plate can be restored in Hspg2$^{-/-}$-Tg mice (Fig. 7B). Type II collagen, type X collagen, and osteopontin expression of Hspg2$^{-/-}$-Tg mice were similar to those of wild-type mice.

Vascular invasion into the chondro-osseous region observed in the Hspg2$^{-/-}$-Tg mice was also similar to that of wild-type mice (Fig. 7D). Since Hspg2$^{-/-}$-Tg mice expressed perlecan in cartridge but not surrounding tissues, these results indicate that the inhibition of vascular invasion in Hspg2$^{-/-}$mice is due to the absence of perlecan in cartilage but not to its absence in endothelial cells.

2.8. Perlecan promotes VEGF-induced VEGFR2 activation in endothelial cells

$VEGF_{164}$ is expressed in hypertrophic chondrocytes and is critical for inducing vascular invasion into the hypertrophic zone (Zelzer et al., 2004). As $VEGF_{164}$ contains a heparan sulfate binding site, perlecan may bind to $VEGF_{164}$, which promotes VEGF signaling of endothelial cells for angiogenesis. We tested the binding of purified perlecan from cartilage to $VEGF_{164}$ in a solid phase binding assay

Please cite this article as: Ishijima, M., et al., Perlecan modulates VEGF signaling and is essential for vascularization in endochondral bone formation, Matrix Biology (2012), doi:10.1016/j.matbio.2012.02.006

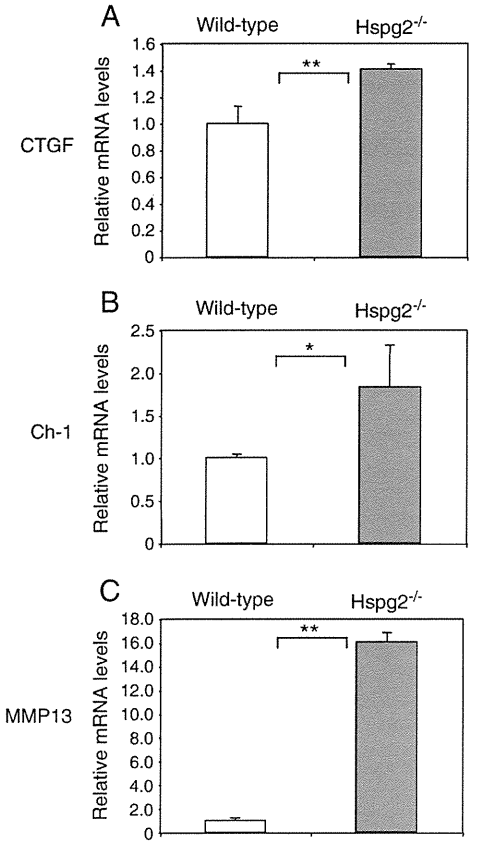

Fig. 5. Expression of molecules involved in vascular invasion. (A, B) Quantitative RT-PCR. Expression of mRNA for the connective tissue growth factor (CTGF) and chondromodulin-1 (Ch-1), which are known to be involved in vascular invasion in endochondral ossification, were significantly increased in chondrocytes from Hspg2$^{-/-}$ mice compared to those in wild-type mice. * and ** indicate $p<0.05$ and <0.01, respectively. **(C)** Expression of MMP13, which is expressed by hypertrophic chondrocytes, was strongly increased in the growth plates of Hspg2$^{-/-}$ mice. **Indicates $p<0.01$.

using perlecan-coated dishes with different amounts of growth factors or growth factor receptors (Fig. 8A). Perlecan bound to FGF2 and to FGF receptors 2 and 3, as reported (Knox et al., 2002; Knox and Whitelock, 2006; Patel et al., 2007; Smith et al., 2007). Perlecan bound to VEGF receptor 2 (VFGFR2), in agreement with recent findings (Goyal et al., 2011). However, perlecan did not bind to $VEGF_{164}$. To test whether perlecan promotes $VEGF_{164}$-mediated VEGFR2 activation, primary endothelial cells from wild-type mouse skin were incubated with $VEGF_{164}$ in the presence of various amounts of perlecan. After being incubated for 5 min at 37 °C, the cells were lysed, and VEGFR2 was immunoprecipitated with anti-VEGFR2 antibody. The proteins were analyzed with Western blotting using anti-pVEGFR2 (Tyr951) and anti-VEGFR2 antibodies as described in the Materials and Methods section. We found that perlecan promoted VEGFR2 phosphorylation (Fig. 8B). The cartilage perlecan-promoted activation of VEGF/VEGFR2 is consistent with the VEGFR2 activation by perlecan from endothelial cells (Zoeller et al., 2009; Goyal et al., 2011).

3. Discussion

Endochondral bone formation occurs through highly coordinated biological processes, including chondrocyte hypertrophy, deposition and remodeling of the cartilage matrix, vascular invasion, apoptosis, osteoblast replacement, and subsequent trabecular bone formation. In this study, we demonstrated that perlecan present in cartilage, but not in capillary basement membranes, is essential for cartilage matrix remodeling, vascular invasion, and the formation of bone marrow and trabecular bone.

Perlecan had been suggested to play crucial roles not only in vasculogenesis but also in the maturation and maintenance of differentiated tissues, including cartilage (Handler et al., 1997). In growth plates of Hspg2$^{-/-}$ mice, the matrix structure is disorganized, and glycosaminoglycans are reduced (Fig. 1A) (Arikawa-Hirasawa et al., 1999; Costell et al., 1999). Biochemical studies in vitro confirmed that perlecan is required for cartilage collagen fibril formation (Kvist et al., 2006). In Hspg2$^{-/-}$ mice, growth plate cartilage is wider, and chondrocytes are located more sparsely in the cartilage matrix than in wild-type mice (Fig. 1). These phenotypes are different from those of cartilage-deficient (cmd/cmd) mice, which are caused by the absence of functional aggrecan, a major chondroitin sulfate proteoglycan in cartilage (Watanabe et al., 1994). These cmd/cmd mice die perinatally; the width of the cartilage of the long bone is narrow, and chondrocytes are rather densely packed in the matrix (Watanabe and Yamada, 2002). In the absence of perlecan, chondrocytes were able to differentiate into mature hypertrophic chondrocytes, which express VEGF (Figs. 3 and 4), MMP13 (Fig. 5C), and osteopontin (Fig. 6B,C). Removal of the hypertrophic matrix and its calcified regions is essential for endochondral bone formation. In wild-type growth plates, only a few layers containing osteopontin and calcification surround mature hypertrophic chondrocytes in the chondro-osseous boundary (Fig. 6). However, in Hspg2$^{-/-}$ growth plates, multiple layers were accumulated near the end of the hypertrophic zone, indicating that hypertrophic cartilage removal was inhibited in the absence of perlecan (Fig. 6). Matrix metalloproteinases, such as MMP-9 and MMP-13, are involved in degradation of the hypertrophic matrix (Vu et al., 1998; Engsig et al., 2000; Inada et al., 2004; Stickens et al., 2004). However, we found that MMP-13 expression was increased in Hspg2$^{-/-}$ growth plates compared to those of wild-type mice. MMP-9 is also expressed in the growth plates of Hspg2$^{-/-}$ mice. Since perlecan interacts with MMPs and is most abundantly expressed in the hypertrophic zone compared with other chondrocyte zones, perlecan may play a role in the activation of MMPs for cartilage remodeling.

Although matrix components are expressed in the cartilage of Hspg2$^{-/-}$ growth plates, the fibrillar formation and density are especially reduced in the hypertrophic zone (Gustafsson et al., 2003). In addition, the columnar structure of hypertrophic chondrocytes is disorganized, and the hypertrophic matrix is often disrupted in Hspg2$^{-/-}$ mice, especially during later stages such as birth (Arikawa-Hirasawa et al., 1999; Costell et al., 1999; Arikawa-Hirasawa et al., 2002). These observations suggest that perlecan provides the strength and rigidity of the hypertrophic matrix structure by interacting with matrix molecules for proper growth plate development. In Hspg2$^{-/-}$ growth plates, the ossified periosteum is formed but apparently curved into the hypertrophic zone, in contrast to the longitudinal growth seen in bone collars of wild-type mice (Fig. 1). Because the formation of bone marrow and the trabecular bone was severely inhibited, the bone collar structure separated two adjacent cartilage molds within the humerus close together (Fig. 1). The abnormal alignment of the bone collar seen in Hspg2$^{-/-}$ growth plates is likely due in part to the less rigid hypertrophic matrix structure.

In addition to MMP-9 and MMP-13, other molecules, such as CTGF (CCN2) and Ch-1, are implicated in matrix remodeling and vascular invasion in the growth plates (Ivkovic et al., 2003). In Hspg2$^{-/-}$ growth plates, the expression levels of CTGF and Ch-1 were significantly increased (Fig. 5). VEGFA plays an important role in angiogenesis for endochondral ossification. Administration of an inhibitor of VEGFA activity in mice reduced vascular invasion into the hypertrophic zone and inhibited endochondral bone formation (Gerber et al.,

Please cite this article as: Ishijima, M., et al., Perlecan modulates VEGF signaling and is essential for vascularization in endochondral bone formation, Matrix Biology (2012), doi:10.1016/j.matbio.2012.02.006

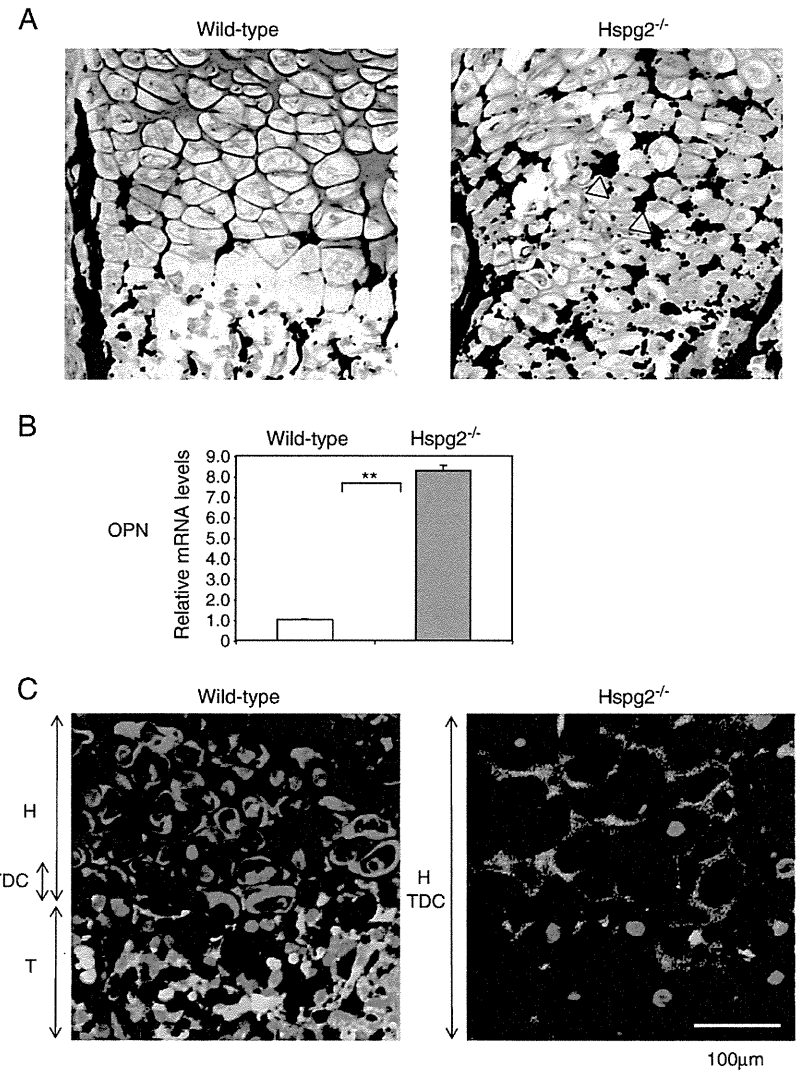

Fig. 6. Accumulation of mature population of hypertrophic chondrocytes in the growth plates of Hspg2$^{-/-}$ mice. **(A)** Double staining of Safranin-O (red) and von Kossa (brown) staining at the proximal end of the humerus in E18.5 wild-type and Hspg2$^{-/-}$ mice. In E18.5 Hspg2$^{-/-}$ mice, the matrix surrounding multiple layers of hypertrophic chondrocytes is calcified, whereas in the wild-type growth plate, the matrix surrounding only a few hypertrophic layers at the end of cartilage is calcified. Arrowheads indicate the formation of hydroxyapatite nodules (calcospherites) in the hypertrophic zone of Hspg2$^{-/-}$ mice. (B) Real-time RT-PCR analysis. Osteopontin OPN mRNA expression was significantly increased in the chondrocytes of E18.5 Hspg2$^{-/-}$ mice compared with the expression in wild-type mice. ** indicates $p<0.01$. **(C)** Double immunostaining for OPN (green) and perlecan (red) of the proximal end of the humerus in E18.5 wild-type and Hspg2$^{-/-}$ mice. OPN-expressing mature hypertrophic chondrocytes accumulated in the growth plates of Hspg2$^{-/-}$ mice. Only a few hypertrophic cell layers expressed OPN in the terminally differentiated chondrocyte area (TDC) of the wild-type mice . Perlecan was expressed in the area of hypertrophic chondrocytes (H) and TDC, but not in the trabecular bone area (T) of the growth plate of wild-type mice. Perlecan was completely absent in all of these areas in Hspg2$^{-/-}$ mice. Scales show 100 μm in length. (For interpretation of the references to color in this figure legend, the reader is referred to the web version of this article.)

1999). Conditional VEGFA knockout in mice specific in chondrocytes using Col2a1Cre displayed an expansion of the hypertrophic zone, delayed vascular invasion, and impaired endochondral ossification (Zelzer et al., 2004). Forced expression of Runx2 in hypertrophic chondrocytes using the Col10a1 promoter reduced VEGFA expression and resulted in impaired cartilage matrix remodeling and an almost complete lack of bone marrow due to the inhibition of vascular invasion into hypertrophic cartilage (Hattori et al., 2010). In the Hspg2$^{-/-}$ growth plates, the VEGF protein levels were increased. $VEGF_{120}$ and $VEGF_{164}$ mRNA were expressed in the growth plates of wild-type mice. The mRNA expression levels for $VEGF_{120}$ and $VEGF_{164}$ were increased in Hspg2$^{-/-}$ growth plates, with the highest level for $VEGF_{164}$ (Fig. 4B). In the zebrafish, perlecan regulates angiogenic blood vessel formation, and perlecan knockdown results in an abnormal increase and relocation of the VEGFA proteins (Zoeller et al., 2009). In wild-type mice, perlecan is expressed not only in cartilage but also in blood vessel basement membranes. We therefore examined whether cartilage or endothelial perlecan is important for normal vascular invasion into the hypertrophic zone and endochondral bone formation by expressing the perlecan (Hspg2) transgene (Tg) specifically in the cartilage of HSPG2$^{-/-}$ mice (Xu et al., 2010). The mutant mice (Hspg2$^{-/-}$-Tg) expressed perlecan in cartilage but not in surrounding tissues (Fig. 7C)(Xu et al., 2010). Hspg2$^{-/-}$-Tg mice survived and showed normal cartilage development and endochondral bone formation (Fig. 7A, B, D). These results suggest that perlecan is critical in cartilage but not in endothelial cell basement membranes for vascular invasion into the hypertrophic zone. Since vascularization in other tissues

Please cite this article as: Ishijima, M., et al., Perlecan modulates VEGF signaling and is essential for vascularization in endochondral bone formation, Matrix Biology (2012), doi:10.1016/j.matbio.2012.02.006

occurred without perlecan, the mechanism of angiogenesis must be unique in endochondral ossification processes.

Perlecan purified from bovine cartilage enhanced the activation of $VEGF_{164}$-VEGFR2 signaling in endothelial cells (Fig. 8). This activation is facilitated via direct binding of perlecan to VEGFR2 (Fig. 8A). Perlecan from endothelial cell culture and recombinant endorepellin, the C-terminal part of perlecan, binds to VEGFR1 and 2 (Goyal et al., 2011). Perlecan promotes angiogenesis, while its fragment acts as an anti-angiogenic factor by disrupting the actin assembly of endothelial cells through interaction with α2β1 integrin (Bix et al., 2004). Endorepellin attenuated VEGFA-mediated activation of VEGFR2 in endothelial cells, and this attenuation is required for α2β1 integrin (Goyal et al., 2011). Cartilage perlecan did not bind to $VEGF_{164}$, while endothelial cell perlecan binds to the heparin-binding site containing VEGFA (Goyal et al., 2011). This difference may be because cartilage perlecan is substituted with not only heparan sulfate chains but also chondroitin sulfate chains, which may inhibit perlecan interactions with $VEGF_{164}$.

Studies by Takimoto et al., (Takimoto et al., 2009), with overexpression of VEGFA in cartilage in transgenic mice and in chick embryonic forelimbs, revealed the perichondrium prevents vascular invasion into cartilage from highly vascularized surrounding tissues at early stages, but at later stages, perichondrial angiogenesis occurs and is followed by vascular invasion into the hypertrophic zone. This process is required for heparin-binding VEGF isoforms. In $Hspg2^{-/-}$ mice, heparin-binding $VEGF_{164}$ was excessively expressed in the hypertrophic zone, and vasculature in the perichondrium and bony collar was observed, but osteoclasts were reduced, and vascular invasion was inhibited (Fig. 2A). Since perlecan is not expressed in the perichondrium (data not shown) (Melrose et al., 2004; Smith et al., 2010), other molecules, such as Nrp1 and Nrp2, which are expressed in the vasculature of surrounding tissues (Takimoto et al., 2009), enhance VEGFR2 signaling via binding to VEGFA as a receptor (Staton et al., 2007; Herve et al., 2008).

In summary, we demonstrated that perlecan in cartilage is essential for vascular invasion from the perichondrium into the hypertrophic zone. We showed that cartilage perlecan enhances VEGF/

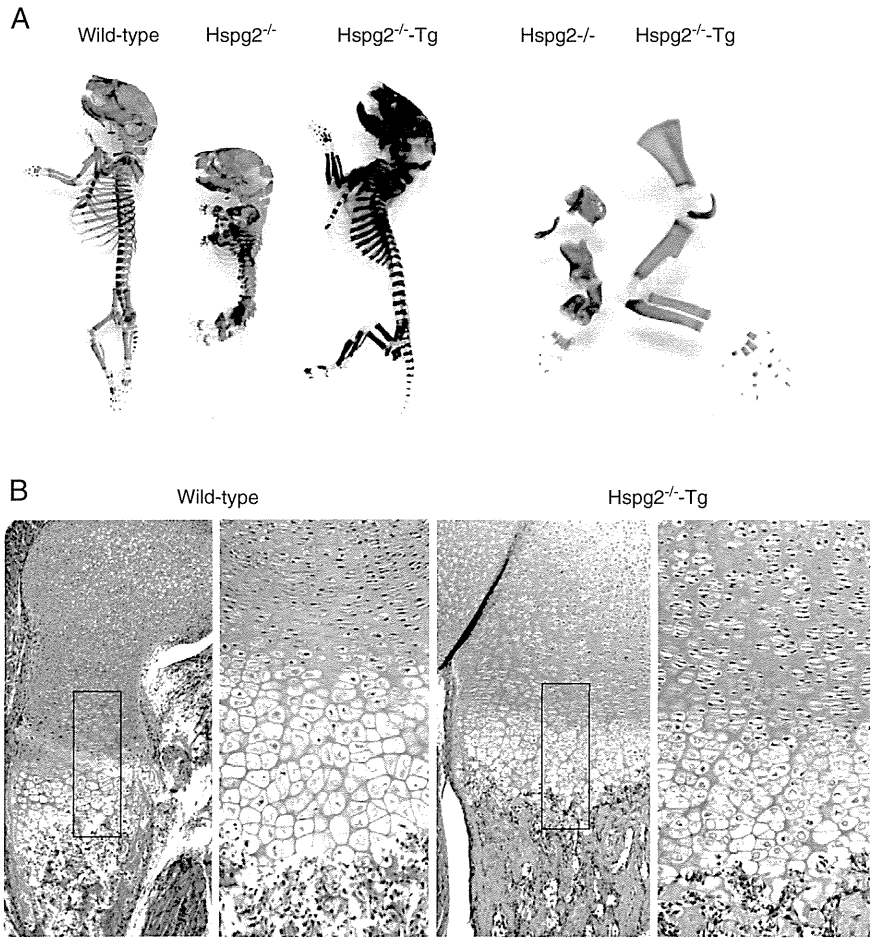

Fig. 7. *Restore skeletal abnormalities of $Hspg2^{-/-}$ mice to normal by mating with transgenic mice (Col2a1-PerTg).* (A) *Skeletal abnormalities of $Hspg2^{-/-}$ mice were rescued by* creating $Hspg2^{-/-}$-Tg mice containing the Hspg2 transgene (Col2a1-PerTg) under the control of a chondrocyte-specific Col2a1 promoter and enhancer. The left three panels show skeletal preparations of E18.5 whole embryos (wild-type, $Hspg2^{-/-}$, and $Hspg2^{-/-}$-Tg); the right two panels show hind limbs from E18.5 $Hspg2^{-/-}$ and $Hspg2^{-/-}$-Tg mice. Cartilage was stained with Alcian blue, and bone was stained with Alizarin red S. (B) Histological sections of the growth plate of E18.5 hind limbs of wild-type mice stained with H-E. Columnar structure of the growth plate was restored in $Hspg2^{-/-}$-Tg mice. (C) Immunostaining of extracellular matrix proteins in E18.5 growth plates from wild-type and $Hspg2^{-/-}$-Tg mice. Perlecan was expressed in the growth plates of $Hspg2^{-/-}$-Tg mice. Expression of type II collagen (Col2), type X collagen (Col10), and osteopontin (OPN) was similar for the wild-type and $Hspg2^{-/-}$-Tg mice. **(D)** Immunostaining of CD31 in the growth plate of E18.5 wild-type and $Hspg2^{-/-}$-Tg mice. The vascular invasion of the chondro-osseous boundary and bone marrow observed in $Hspg2^{-/-}$-Tg mice was similar to that in wild-type mice.

Please cite this article as: Ishijima, M., et al., Perlecan modulates VEGF signaling and is essential for vascularization in endochondral bone formation, Matrix Biology (2012), doi:10.1016/j.matbio.2012.02.006

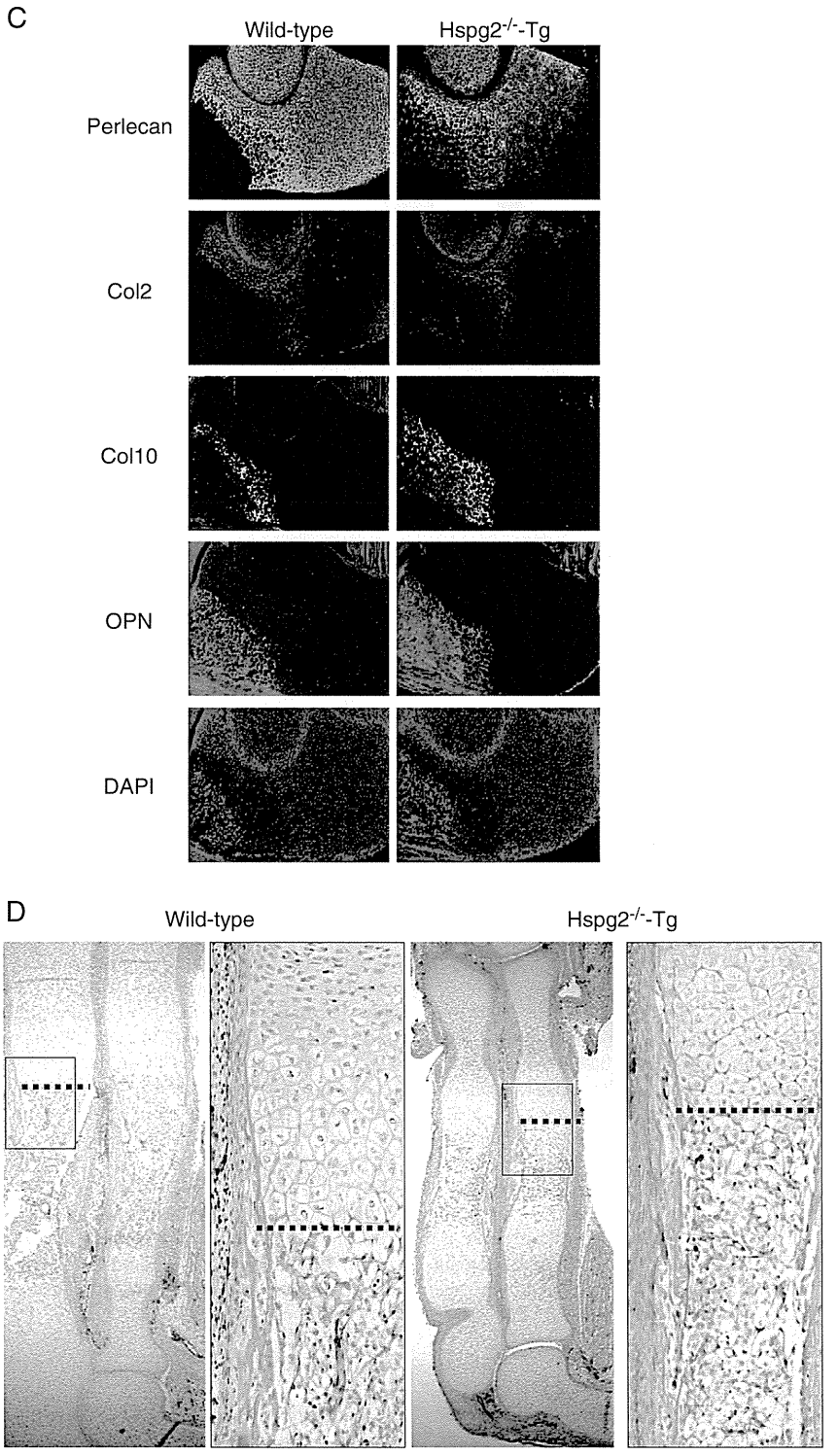

Fig. 7 (*continued*)

VEGFR signaling of endothelial cells in culture. In Hspg2$^{-/-}$ growth plates, hypertrophic chondrocytes express molecules such as MMP-13, OPN, CTGF, and VEGFA, which are important for cartilage matrix remodeling and for vascular invasion. However, without perlecan in cartilage, the osteopontin-expressing hypertrophic chondrocyte layers and calcified areas expand, and formation of bone marrow and the trabecular bone is inhibited. The defect in vascular invasion results in the inhibition of cartilage remodeling and replacement of

Please cite this article as: Ishijima, M., et al., Perlecan modulates VEGF signaling and is essential for vascularization in endochondral bone formation, Matrix Biology (2012), doi:10.1016/j.matbio.2012.02.006

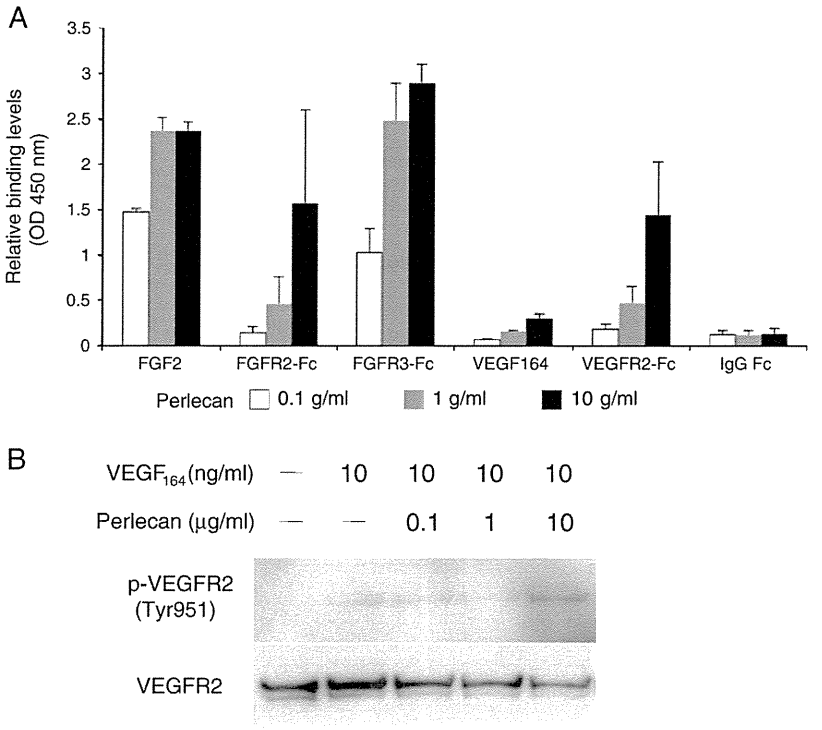

Fig. 8. Perlecan binds to VEGFR2 and promotes VEGF-induced VEGFR2 activation in endothelial cells. Binding of cartilage perlecan to FGF2 and $VEGF_{164}$ and their receptors at various concentrations in solid phase assays. Perlecan bound to FGF2 and FGFR2. Perlecan did not bind to $VEGF_{164}$ but bound to its receptor, VEGFR2. (B) Western blots of VEGFR2 and phosphorylated VEGFR2 of endothelial cells treated with $VEGF_{164}$ and perlecan. Perlecan promoted the phosphorylation levels of VEGFR2 in the presence of VEGFA.

hypertrophic chondrocytes with osteoblasts, which leads to severe defects in endochondral bone formation of $Hspg2^{-/-}$ mice.

4. Experimental procedures

4.1. Mice

Perlecan knockout ($Hspg2^{-/-}$) mice were generated as described previously (Arikawa-Hirasawa et al., 1999). About half of the $Hspg2^{-/-}$ mice died around embryonic day (E) 10 of hemorrhage due to defective myocardium basement membranes (Arikawa-Hirasawa et al., 1999; Costell et al., 1999; Xu et al., 2010). Perinatal lethality-rescued perlecan knockout mice ($Hspg2^{-/-}$-Tg, $Hspg2^{-/-}$; Col2a1-$Hspg2^{Tg/-}$) were created by expressing a transgene for perlecan under the control of the Col2a1 promoter and enhancer specifically to cartilage (Col2a1-PerTg) in $Hspg2^{-/-}$ mice (Xu et al., 2010). The animal protocol approved by the NIDCR ACU Committee was used for maintaining and handling mice, and all mice were housed in a mouse facility affiliated with the American Association for the Accreditation of Laboratory Animal Care.

4.2. Skeletal histology

Paraffin sections (5 μm) of mouse embryos were deparaffinized using xylene, rehydrated through an alcohol gradient series to water, and then used for histological and immunohistochemical analysis. Paraformaldehyde (4%) was used for fixation in histology and immunohistochemistry. Double staining for Safranin-O and von Kossa staining was performed as described (Aszodi et al., 2003). Immunostaining was performed using a Histostain-SP kit (Zymed) according to the manufacturer's instructions. The following antibodies were used for immunohistochemical studies: a rabbit polyclonal antibody for perlecan from Dr. T. Sasaki (University of Erlangen-Nuremberg, Erlangen, Germany), a monoclonal antibody for osteopontin (R&D Systems), a monoclonal antibody for VEGF (R&D Systems), a monoclonal antibody for type II collagen (Hybridoma Bank, University of Iowa), and a type X collagen chain from Greg Lunstrum (Shriners Hospital for Children Research Center, Portland). Immunostaining for CD31 was performed using a monoclonal antibody for CD31 (Pharmingen) as described previously (Colnot et al., 2005). For the immunofluorescence study, fluorescein isothiocyanate (FITC)-conjugated or Alexa-488-conjugated (Jackson ImmunoResearch Laboratories) was used as a secondary antibody. Tartrate-resistant acid phosphatase (TRAP) was stained as described previously (Ishijima et al., 2001, 2007).

4.3. Skeletal analysis

Bones and cartilage of newborn mice were stained with Alizarin red and Alcian blue as described previously (Arikawa-Hirasawa et al., 1999). The bone length and width were histologically measured, and the relative length and width of the humeri in the wild-type mice were set at 100%.

4.4. RT-PCR analysis

Total RNA was extracted from growth plate cartilage of the distal end of the femora and the proximal end of the tibiae of E16.5 or E18.5 embryos using TRIzol (Invitrogen).

For reverse transcription, 2 μg of total RNA were used to generate cDNA, which was used as a template for PCRs with gene-specific primers. cDNA was amplified with an initial denaturation at 95 °C for 3 min, and then at 95 °C for 30 s, 60 °C for 30 s, and 72 °C for 30 s for 25 cycles. A final elongation step was conducted at 72 °C for 5 min, and then the cDNA was separated on agarose gels. Real-time PCR analysis was performed using a TaqMan Real-Time PCR detection system (ABI7000,

Please cite this article as: Ishijima, M., et al., Perlecan modulates VEGF signaling and is essential for vascularization in endochondral bone formation, Matrix Biology (2012), doi:10.1016/j.matbio.2012.02.006

Applied Biosystems). TaqMan Universal Master Mix and TaqMan Gene Expression Assays Hs99999901_s1 and Hs01078483_g1 (Applied Biosystems) were used according to the manufacturer's protocol, with a final reaction volume of 25 μl. Sequences for VEGF-120, -164, -188, CTGF, Ch-1, MMP13, and OPN specific PCR primers are available from the authors upon request.

4.5. Western blotting

Growth plate cartilage of the distal end of the femora and the proximal end of the tibiae of E16 mice was dissected from the right side of the knee joint and then lysed. The lysates were run on a 10% SDS-PAGE. A monoclonal antibody for VEGF (C-1, Santa Cruz) was used for Western blot analysis.

For the phosphorylation assay of VEGFR2, primary endothelial cells were prepared from the wild-type mouse skin at postnatal day 4 by immunopanning using anti-ICAM2 antibody (BD Biosciences), as described previously (Kataoka et al., 2003). The endothelial cells were cultured in DMEM: F12 = 1:1 (Invitrogen) containing 100 μM nonessential amino acid (Invitrogen), 20% fetal calf serum (FCS; Hyclone), 100 μg/ml heparin (Sigma-Aldrich), 100 U penicillin (Invitrogen), 100 μg/ml streptomycin (Invitrogen), and 50 μg/ml endothelial cell growth supplement (ECGS; BD Biosciences). For starvation of the phosphorylation assay, FCS, heparin, and ECGS were eliminated from the medium, and endothelial cells were incubated overnight. $VEGF_{164}$ and various amounts of perlecan were mixed and preincubated at room temperature for 1 h. After preincubation, the mixture of $VEGF_{164}$ and perlecan was added to the starved endothelial cell culture, and the cells were incubated for 5 min at 37 °C. The cells were lysed with the lysis buffer (1% Triton-X100, 1.5 mM EDTA, 1 mM Na_3PO_4, 25 mM NaF, and 1 mM Na_3VO_4 in Tris-buffered saline) for 5 min on ice. The cell lysate was centrifuged at 15,000 rpm for 30 min at 4 °C and separated from the cell pellet. Fifty μg of the cell lysate was incubated with anti-VEGFR2 antibody (Cell Signaling) in the binding/washing buffer (0.1% Triton-X100, 1.5 mM EDTA, 1 mM Na_3PO_4, 25 mM NaF, and 1 mM Na_3VO_4 in Tris-buffered saline) for 1 h at 4 °C. Then, protein-G Sepharose beads (Invitrogen) were added to the reaction mixture and incubated for 1 h at 4 °C. After incubation, the beads were washed with the binding/washing buffer. Proteins bound to the beads were eluted with the LDS-sample buffer (Invitrogen) with 10 μM DTT. The proteins were detected with Western blotting using anti-pVEGFR2 (Tyr951) and anti-VEGFR2 antibodies (Cell Signaling).

4.6. Binding assays

A solid phase binding assay was performed using purified perlecan from bovine cartilage (Govindraj et al., 2002). Two hundred and fifty ng of perlecan was coated onto 96-well plates at 4 °C overnight. The wells were blocked with the blocking buffer (3% bovine serum albumin: Sigma-Aldrich) at room temperature for 2 h. After blocking, various amounts of FGF-basic (PeproTech), $VEGF_{164}$ (R&D Systems), and recombinant fusion proteins of extracellular domains of FGFR2, FGFR3, and VEGFR2 with the human IgG Fc portion (R&D Systems) in the blocking buffer were added and incubated at room temperature for 1 h. The proteins bound to perlecan were detected with anti-FGF-basic (Millipore), anti-VEGF (Santa Cruz Biotech.), biotinylated anti-human IgG (Jackson ImmunoResearch Inc.), and horseradish peroxidase (HRP)-conjugated secondary antibodies (Thermo) and streptavidin (Sigma-Aldrich). After incubation with appropriate antibodies, 3,3',5,5'-tetramethyl-benzidine solution (Sigma-Aldrich) was added to the wells and incubated for 10 min at room temperature. After 0.5 N H_2SO_4 was added to stop the colorimetric reaction by HRP, the optical density at 450 nm was measured using a microplate reader (Safire, Tecan Ltd.).

4.7. Statistical analysis

Group means were compared with analysis of variance, and the significance of differences was determined by using an unpaired *t*-test. *P* values less than 0.05 were considered significant.

Acknowledgments

This work was supported by the Intramural Program of the NIDCR, NIH (Y.Y.), and grant-in-aid (to 19791047 and 21791418 for M.I and 22300223 for E.A-E) from the Ministry of Education, Science, and Culture of Japan. M.I., N.S., K.H., and T.M. were supported in part by a fellowship from the Japan Society for the Promotion of Science.

References

Arikawa-Hirasawa, E., Watanabe, H., Takami, H., Hassell, J.R., Yamada, Y., 1999. Perlecan is essential for cartilage and cephalic development. Nat Genet 23, 354–358.

Arikawa-Hirasawa, E., Wilcox, W.R., Le, A.H., Silverman, N., Govindraj, P., Hassell, J.R., Yamada, Y., 2001a. Dyssegmental dysplasia, Silverman–Handmaker type, is caused by functional null mutations of the perlecan gene. Nat Genet 27, 431–434.

Arikawa-Hirasawa, E., Wilcox, W.R., Yamada, Y., 2001b. Dyssegmental dysplasia, Silverman–Handmaker type: unexpected role of perlecan in cartilage development. Am J Med Genet 106, 254–257.

Arikawa-Hirasawa, E., Le, A.H., Nishino, I., Nonaka, I., Ho, N.C., Francomano, C.A., Govindraj, P., Hassell, J.R., Devaney, J.M., Spranger, J., Stevenson, R.E., Iannaccone, S., Dalakas, M.C., Yamada, Y., 2002. Structural and functional mutations of the perlecan gene cause Schwartz–Jampel syndrome, with myotonic myopathy and chondrodysplasia. Am J Hum Genet 70, 1368–1375.

Aszodi, A., Hunziker, E.B., Brakebusch, C., Fassler, R., 2003. Beta1 integrins regulate chondrocyte rotation, G1 progression, and cytokinesis. Genes Dev 17, 2465–2479.

Aviezer, D., Hecht, D., Safran, M., Eisinger, M., David, G., Yayon, A., 1994. Perlecan, basal lamina proteoglycan, promotes basic fibroblast growth factor-receptor binding, mitogenesis, and angiogenesis. Cell 79, 1005–1013.

Bix, G., Fu, J., Gonzalez, E.M., Macro, L., Barker, A., Campbell, S., Zutter, M.M., Santoro, S.A., Kim, J.K., Hook, M., Reed, C.C., Iozzo, R.V., 2004. Endorepellin causes endothelial cell disassembly of actin cytoskeleton and focal adhesions through alpha2beta1 integrin. J Cell Biol 166, 97–109.

Brandau, O., Aszodi, A., Hunziker, E.B., Neame, P.J., Vestweber, D., Fassler, R., 2002. Chondromodulin I is dispensable during enchondral ossification and eye development. Mol Cell Biol 22, 6627–6635.

Brown, J.C., Sasaki, T., Gohring, W., Yamada, Y., Timpl, R., 1997. The C-terminal domain V of perlecan promotes beta1 integrin-mediated cell adhesion, binds heparin, nidogen and fibulin-2 and can be modified by glycosaminoglycans. Eur J Biochem 250, 39–46.

Colnot, C., de la Fuente, L., Huang, S., Hu, D., Lu, C., St-Jacques, B., Helms, J.A., 2005. Indian hedgehog synchronizes skeletal angiogenesis and perichondrial maturation with cartilage development. Development (Cambridge, England) 132, 1057–1067.

Costell, M., Gustafsson, E., Aszodi, A., Morgelin, M., Bloch, W., Hunziker, E., Addicks, K., Timpl, R., Fassler, R., 1999. Perlecan maintains the integrity of cartilage and some basement membranes. J Cell Biol 147, 1109–1122.

DeCarlo, A.A., Whitelock, J.M., 2006. The role of heparan sulfate and perlecan in bone-regenerative procedures. J Dent Res 85, 122–132.

Engsig, M.T., Chen, Q.J., Vu, T.H., Pedersen, A.C., Therkidsen, B., Lund, L.R., Henriksen, K., Lenhard, T., Foged, N.T., Werb, Z., Delaisse, J.M., 2000. Matrix metalloproteinase 9 and vascular endothelial growth factor are essential for osteoclast recruitment into developing long bones. J Cell Biol 151, 879–889.

Gerber, H.P., Vu, T.H., Ryan, A.M., Kowalski, J., Werb, Z., Ferrara, N., 1999. VEGF couples hypertrophic cartilage remodeling, ossification and angiogenesis during endochondral bone formation. Nat Med 5, 623–628.

Ghiselli, G., Eichstetter, I., Iozzo, R.V., 2001. A role for the perlecan protein core in the activation of the keratinocyte growth factor receptor. Biochem J 359, 153–163.

Govindraj, P., West, L., Koob, T.J., Neame, P., Doege, K., Hassell, J.R., 2002. Isolation and identification of the major heparan sulfate proteoglycans in the developing bovine rib growth plate. J Biol Chem 277, 19461–19469.

Govindraj, P., West, L., Smith, S., Hassell, J.R., 2006. Modulation of FGF-2 binding to chondrocytes from the developing growth plate by perlecan. Matrix Biol 25, 232–239.

Goyal, A., Pal, N., Concannon, M., Paul, M., Doran, M., Poluzzi, C., Sekiguchi, K., Whitelock, J.M., Neill, T., Iozzo, R.V., 2011. Endorepellin, the angiostatic module of perlecan, interacts with both the alpha2beta1 integrin and vascular endothelial growth factor receptor 2 (VEGFR2): a dual receptor antagonism. J Biol Chem 286, 25947–25962.

Gustafsson, E., Aszodi, A., Ortega, N., Hunziker, E.B., Denker, H.W., Werb, Z., Fassler, R., 2003. Role of collagen type II and perlecan in skeletal development. Ann N Y Acad Sci 995, 140–150.

Handler, M., Yurchenco, P.D., Iozzo, R.V., 1997. Developmental expression of perlecan during murine embryogenesis. Dev Dyn 210, 130–145.

Hattori, T., Muller, C., Gebhard, S., Bauer, E., Pausch, F., Schlund, B., Bosl, M.R., Hess, A., Surmann-Schmitt, C., von der Mark, H., de Crombrugghe, B., von der Mark, K., 2010. SOX9 is a major negative regulator of cartilage vascularization, bone marrow

Please cite this article as: Ishijima, M., et al., Perlecan modulates VEGF signaling and is essential for vascularization in endochondral bone formation, Matrix Biology (2012), doi:10.1016/j.matbio.2012.02.006